8-27-2012

A geodesic finite-difference time-domain model of magnetized plasma

Ryan Schlegel

Follow this and additional works at: https://digitalrepository.unm.edu/ece_etds

Recommended Citation

Ryan Schlegel
Candidate

Electrical and Computer Engineering
Department

This thesis is approved, and it is acceptable in quality and form for publication:

Approved by the Thesis Committee:

Dr. Mark A. Gilmore, Chairperson

Dr. Jamesina J. Simpson

Dr. Edward D. Graham, Jr.

Dr. Luke F. Lester

**A GEODESIC FINITE-DIFFERENCE TIME-DOMAIN MODEL
OF MAGNETIZED PLASMA**

by

RYAN SCHLEGEL

**BACHELOR OF SCIENCE IN ELECTRICAL
ENGINEERING**

THESIS

Submitted in Partial Fulfillment of the
Requirements for the Degree of

**Master of Science
Electrical Engineering**

The University of New Mexico
Albuquerque, New Mexico

July, 2012

A GEODESIC FINITE-DIFFERENCE TIME-DOMAIN MODEL OF MAGNETIZED IONOSPHERIC PLASMA

by

Ryan Schlegel

B.S., Electrical Engineering, New Mexico Institute of Mining and Technology

M.S., Electrical Engineering, University of New Mexico, 2012

ABSTRACT

Electromagnetic wave propagation in the Earth-ionosphere cavity presents an interesting challenge for simulations. Three-dimensional latitude-longitude finite-difference time-domain (FDTD) models accounting for the bathymetry, topography and ionosphere have been developed and applied towards a number of applications previously. However, to date most of these models treat the ionosphere as a simple, isotropic exponential conductivity profile. Only recently has a latitude-longitude FDTD model been developed that treats the ionosphere as a magnetized cold plasma. This opens the door to modeling electromagnetic phenomena at higher frequencies and higher altitudes by accommodating more physics. Further, a geodesic (hexagonal-pentagonal) FDTD model that is more efficient, is easier to implement, and executes faster than latitude-longitude models has been recently developed. In this thesis, the magnetized cold plasma global latitude-longitude algorithm is adapted and implemented for the first time in a geodesic FDTD model of the Earth-ionosphere cavity.

Table of Contents

List of Figures

Chapter 1

Introduction

1.1 Modeling the Earth-Ionosphere System Using FDTD

Modeling of the Earth-Ionosphere system using finite-difference time-domain, FDTD [1] is a challenging problem to solve. [2] contains a detailed history of the method. In 1999, Thevenot et al published a paper combining the current density equations of the Ionosphere with Maxwell's equations, creating a 2D FDTD simulation that took into account the Earth's magnetic field [3]. The results from their paper matched existing waveguide models of the Earth-Ionosphere, but the model had strict requirements on the choice of time step to maintain stability [3].

This was followed by Cummer's work in 2000 comparing existing mode theory solutions to the Earth-Ionosphere with a new model using 2D FDTD [4] to model ELF wave propagation generated by lightning strikes. Cummer treated the Ionosphere as an inhomogeneous and anisotropic cold plasma using equations from [5]. He found that mode theory and FDTD produced similar results over the extremely low frequency (ELF) and very low frequency (VLF) ranges, 3 Hz to 300 Hz and 3 kHz to 30 kHz respectively, with the exception of distance less then 2 km from the source [5]. At these distances, mode theory becomes less accurate as it does not account for evanescent waves near the source or waves created by post-discharge currents in the Ionosphere. However, these types of effects are handled inherently by FDTD models without the need for special cases.

These papers demonstrated the possibility for FDTD models to simulate Earth-Ionosphere cavity effects on ELF waves. However, the previous models have been 2D and the uses for such models are limited. Continuing work in the field has moved into 3D Earth-Ionosphere FDTD models.

1.2 Latitude-Longitude Grid FDTD Model

In 2003, Simpson and Taflove used a global Latitude-Longitude grid spherical coordinate FDTD

simulation to model impulsive ELF propagation [6]. In this model, the grid is divided into two modes, transverse electric (TE) and transverse magnetic (TM) propagating modes. Each mode has a separate set of cells, each offset by half a cell. This system allows for ELF propagation in the Earth-Ionosphere cavity and accounts for geometrical and electrical inhomogeneities from the Ionosphere, Lithosphere, and oceans [6]. However, this was largely a validation study and did not include details of the derivation of the grid.

In 2004, Simpson and Taflove expanded on their 2003 validation study and provided greater details on the 3D Latitude-Longitude mesh. In [7], it is shown that isosceles trapezoidal cells as well as isosceles triangular cells are used to grid the Earth-Ionosphere system as seen in Figure 1.
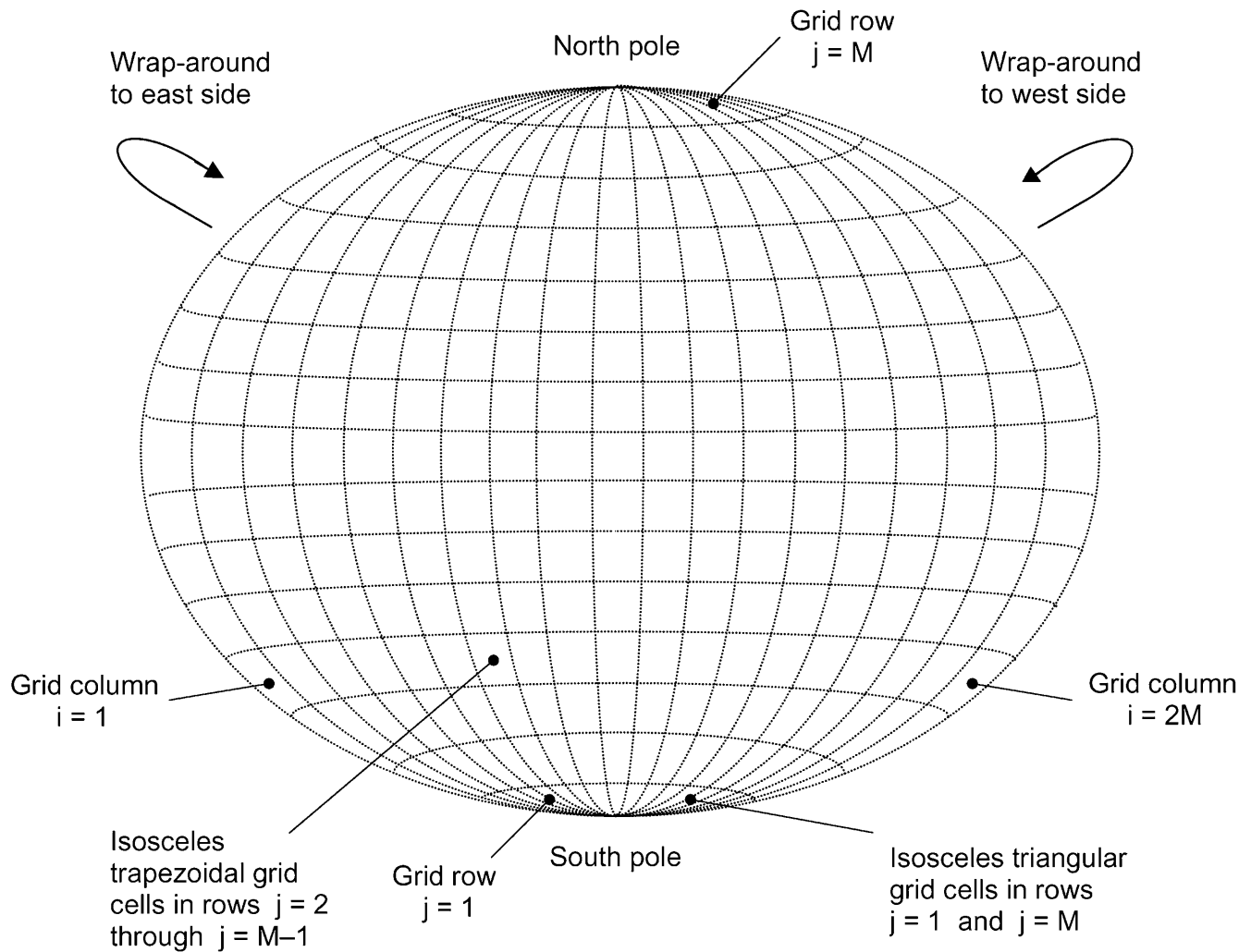
Figure 1: General 3D FDTD Grid as Seen in a TM Plane at a Constant Radial Coordinate [7]

As stated above, the system is separated into two planes, TM and TE. In the TM plane, each cell consists of either a trapezoid or a triangle with the latter being used at cells near the poles. At the center of each cell is a radial Ez component of the propagating field. On each side of this cell is a non-radial component of the magnetic field. This can be seen in Figure 2.
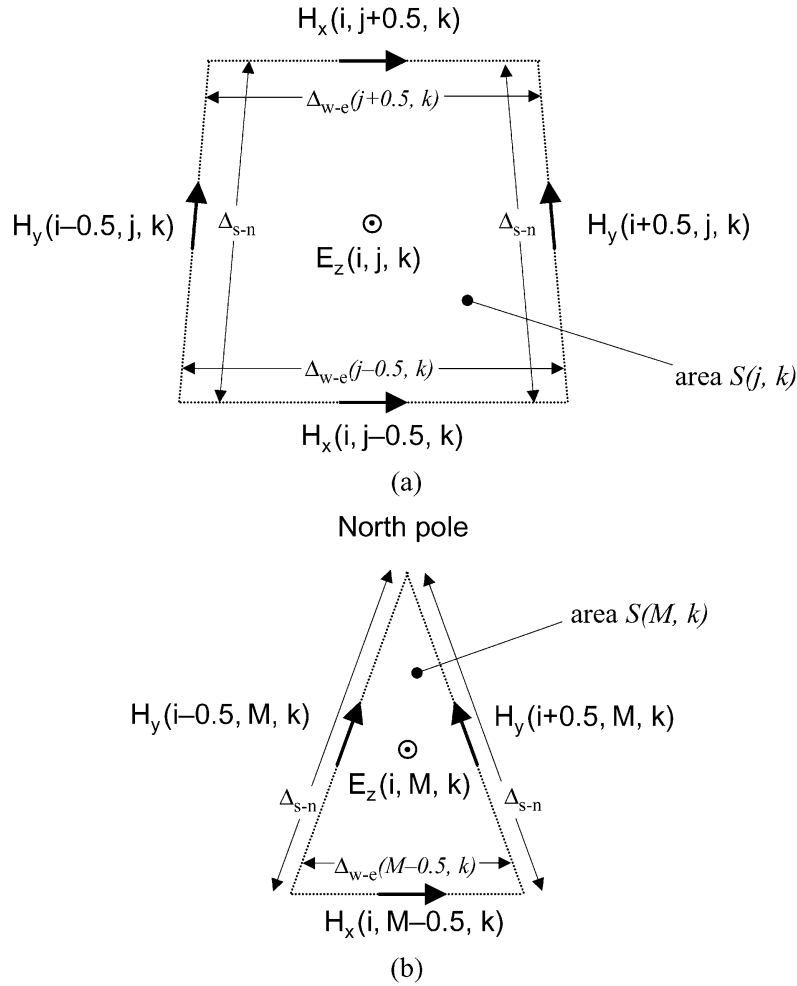
Figure 2: TM Plane Cell Geometry [7]

A half cell above (k + ½), northward (j + ½), and eastward (i + ½) lies the TE plane. The cell geometry is similar, with a radial Hz component in the center of each cell and the non-radial electric fields on the edges. Applying Maxwell's equations to these cells provides an updating equation for each field component. This process is shown in detail in section 2.1 for a rectangular system.

Cells at the equator will be the largest and get progressively smaller as they approach the polar regions. This reduces the numerical stability and efficiency of the model. As the cell size decreases, the time step decreases. This lowers the overall execution of the model. However, to combat this problem, Simpson and Taflove used a cell merging technique to eliminate small cells near the poles, increasing the maximum allowable time step [7].

This new 3D model also accounts for topographic and bathymetric data released by the National Oceanic and Atmospheric Administration (NOAA). This data was used to model the Earth-Ionosphere cavity at a depth of ± 100 km of sea level with a mesh size of 40 x 40 x 5 km at the cells at the equator using the conductivity profile shown in Figure 3 for the Earth's crust [7]. The model also used an exponential conductivity profile presented in [8] by Bannister for the profile of the Ionosphere. The model was then excited using a Gaussian pulse at the surface to a height of 5 km at the equator and 47° W. The result was compared to experimental data of ELF propagation in [9]. Simpson and Taflove found that their results matched the data in [9] to ± 0.5 dB/Mm along a path from the source to a point halfway to the antipode eastward, and ± 1.0 dB/Mm along a similar path but westward [7].
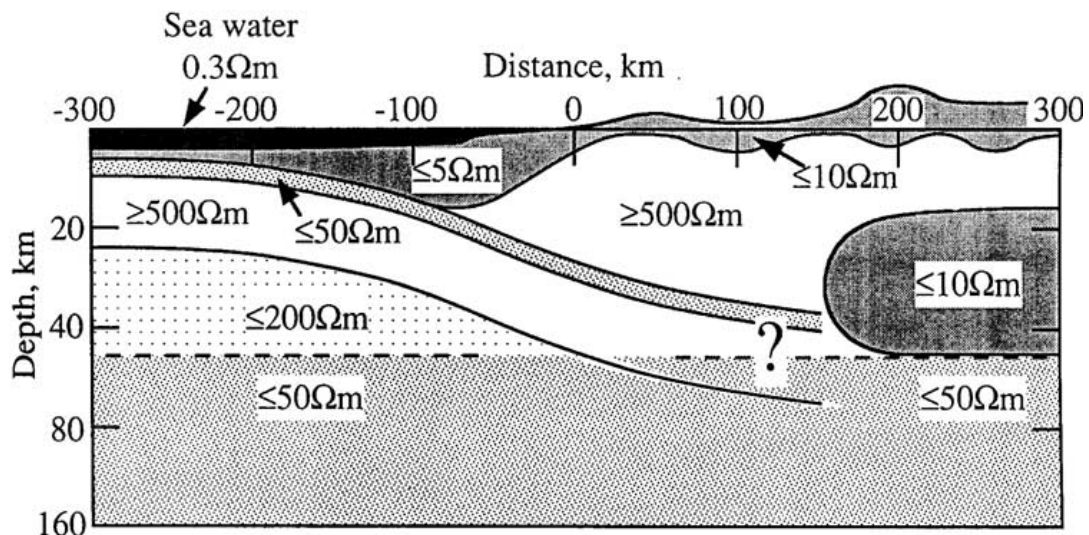
Figure 3: Conductivity Values Used for the Lithosphere According to Whether the Space Lattice Point is Located Directly Below an Ocean or Within a Continent [7]

The level of detail provided by this model was quite extensive. Simpson and Taflove were

4

successful in accounting for topographic, bathymetric, and Ionospheric details in their model while limiting numerical instability. However, this model was further improved upon in [10].

1.3   Latitude-Longitude grid FDTD Model Using a Magnetized Cold Plasma

The Latitude-Longitude grid model accounted for the Ionosphere by using an exponential conductivity profile, but Cummer showed in [4] that the Ionosphere can be treated as a magnetized cold plasma. Yu and Simpson combined Cummer's 2D magnetized cold plasma model with the 3D Latitude-Longitude grid model to further improve the accuracy for ELF waves. Yu and Simpson began with the same equations as Cummer and applied them to the 3D Latitude-Longitude grid producing a system that accounts for the presence of electron, positive ion, and negative ion plasma species. The derivation for this system is covered in detail in sections 2.2 and 2.3, or in the source material [10].

The resulting model was validated by testing the Faraday rotation effect. The Faraday rotation effect occurs in plasma when a magnetic field is applied parallel to a linearly polarized plane wave. This plane wave can be deconstructed into two circularly polarized waves, one right-hand circularly polarized, and the other left-hand circularly polarized. However, in the presence of the parallel magnetic field, the two circular waves will have different phase velocities [11]. This causes the plane of polarization to rotate around the axis of propagation as the wave propagates in the medium [11]. This effect is well documented in plasma theory books such as [11] and [5].

The model used a loss-less electron plasma without ions [4] to test the Faraday rotation effect. The model compared the analytical Faraday rotation angle with the simulated value. The results were in very close agreement with an error of 0.0031% [4].

1.4   Geodesic FDTD

In 2006, Simpson and Taflove developed another 3D FDTD model. Rather then use the Latitude-Longitude grid, they chose a geodesic grid that was being used for climate modeling. The grid used a

mesh consisting of hexagonal and pentagonal cells [12]. Hexagonal cells are used to cover the Earth-Ionosphere cavity, however, hexagonal cells alone cannot completely cover a sphere. A minimum of 12 pentagonal cells are need to complete the grid. Figure 4 is a good representation of the grid, although it contains only a fraction of the cells used in [12]. As in the Latitude-Longitude grid, the TE and TM cases are separated into different cases.
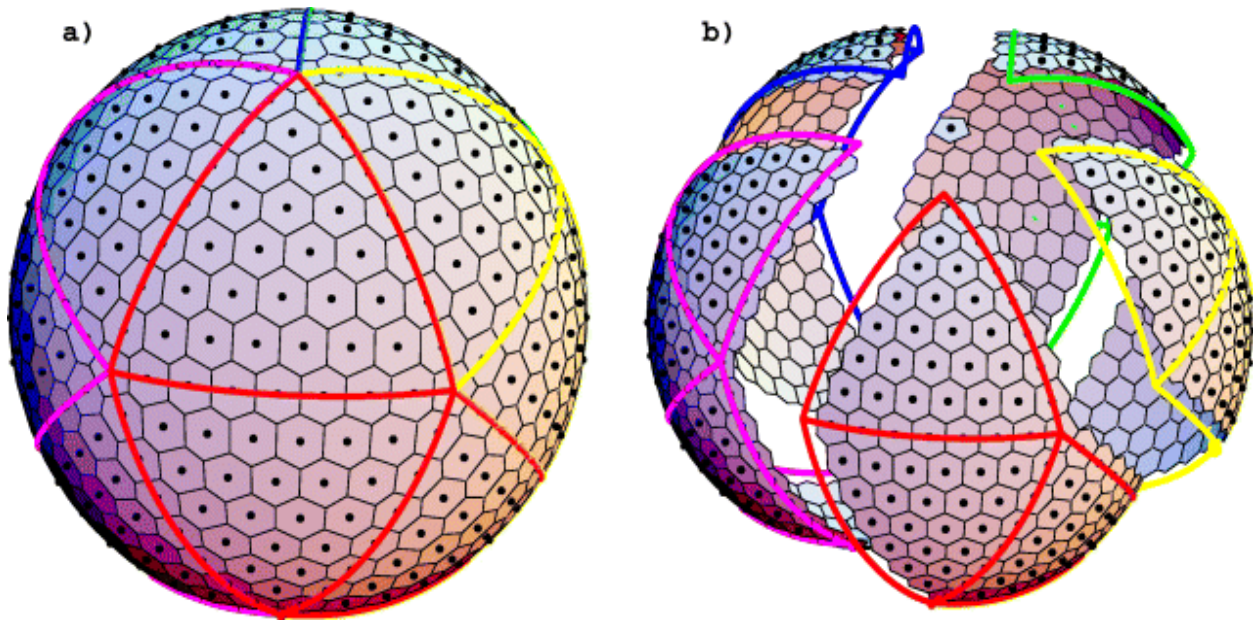
Figure 4: Geodesic Model of a Sphere Using Geodesic Cells [12]

The hexagonal cells are used in the TM mode. In this mode, each cell has a radial Er component located at the center of the cell and six magnetic components located on the edges of the cell. This can be seen in Figure 6. Half a step above the hexagonal cells, k + ½, is another grid consisting of triangles. This is the TE mode and can be seen in Figure 7. At the center of each triangle is a radial Hr component and electric fields along the edges of the cells. Using this mesh, Maxwell's equations were applied to the grid and a system of updating equations was created. As with their Latitude-Longitude grid, Simpson and Taflove used the topographic and bathymetric data from [13] and the Ionosphere conductivity profile from [8] in their model to increase accuracy.

Using this system, Simpson and Taflove performed a test similar to the Latitude-Longitude grid.

They created a mesh of the Earth to a depth of ± 100 km of sea level. This required the use of 163, 842 cells at each radial point [12]. They gave the mesh a resolution of 63 km between grid centers. They also used 40 grid cells in the radial direction giving a resolution of 5 km. In all, the mesh contained over 6.5 million cells [12]. They introduced a Gaussian pulse at the same location, sea level to a 5 km height on the equator and 47° W. Again, they compared the result to experimental data from [9]. The results yielded propagation attenuation values within ± 0.5 dB/Mm from the source along a path halfway to the antipode both eastward and westward [12]. These results are very similar to the results previously obtained in the Latitude-Longitude grid [7]. However, the geodesic model obtained these results 14 times faster with a 40% increase in required memory [12]. It also avoids the time step limitations of the Latitude-Longitude model since cells are of a fixed size and does not require cell merging near the poles. This model shows clear benefits making it an ideal choice for future work.

1.5   Geodesic FDTD Using a Magnetized Cold Plasma

The Latitude-Longitude grid with plasma updates provided a very accurate model for ELF wave propagation in the Earth-Ionosphere cavity. The geodesic model provides the same accuracy as Simpson's Latitude-Longitude grid at a fraction of the run time. Using the geodesic grid in lieu of the Latitude-Longitude grid and applying plasma updates presents clear benefits in computation time with a small increase in memory requirements.

Currently, there are few FDTD implementations on geodesic grids, though a few other researchers have also created their own geodesic grids. In [14] and [15], Wang et al have developed a geodesic grid to analyze the propagation of ELF waves in the Earth-Ionosphere cavity. The model they have developed in [9] shows a field distribution very similar to that used in [12], with radial Er components in the center of hexagonal cells and radial Hr components in the center of triangular cells half a cell above. To validate their model, they excited their model with a Gaussian pulse. A grid size of 10,240

cells at each radial coordinate was used yielding a resolution of 250 km between grid centers [15]. 28 grid cells were used in the radial direction with a resolution of 5 km to grid an area of 40 km below sea level up to 100 km above sea level [15]. This created a grid much coarser then the grid Taflove and Simpson used in [12]. Wang et al compared their FDTD results to [8] as well and found them to be "very close" [15].

Chapter 2

Background

2.1 Finite-Difference Time-Domain (FDTD)

Amongst numerical methods used for modeling electromagnetic waves, FDTD is relatively simple to implement. Since it is a time-domain method, it has a very good response in the frequency domain. Due to the way the FDTD method discretizes problems, it is possible to parallelize an FDTD grid relatively simply. This can make it a good choice if computer clusters or supercomputers are available. FDTD is also very flexible; complex phenomena such as evanescent waves are handled intrinsically in FDTD models and do not require special cases [4].

There have been a multitude of uses for electromagnetic models of the Earth. One use has been a possible earthquake predictor. There are several possible EM precursors that could be used to improve seismic predictions. These include piezomagnetic effects and electrokinetic effects [16]. While these effects could be seismic predictors, data remains inconclusive and require further analysis [11].

In [17], Simpson used FDTD to simulate an Earth-Ionosphere cavity to model electrokinetic currents. Using such a model accounts for lithospheric effects and reverberation [17] [18]. Simpson modeled electrokinetic currents at a depth of 2.5 km and 17 km from the hypocenter of the Loma Prieta earthquake. The model was a qualitative match to data recorded in [19], but had some uncertainties due to insufficient knowledge of the exact lithosphere conductivity instrumentation artifacts in measured data [17].

Global EM modeling has also been used as a means of developing new methods of detecting underground resource formations. In [10] and [12], Simpson developed an FDTD model to detect possible oil fields using a 20 Hz pulse and measuring the radial magnetic field. The magnetic field varied strongly with the conductivity anomalies of the Lithosphere. Simpson used this to propose a

quick and inexpensive method for detecting oil fields using SQUID magnetometers synchronized with 20 Hz pulses [12].

The FDTD method is implemented using the Yee algorithm [20]. Each electric field has four adjacent magnetic fields as can be seen in Figure 5. These magnetic fields are used to calculate the electric field at each point in space using central differencing. In turn, each magnetic field is surrounded by four electric fields which can be used to calculate the magnetic fields by, again, using central differencing [1].
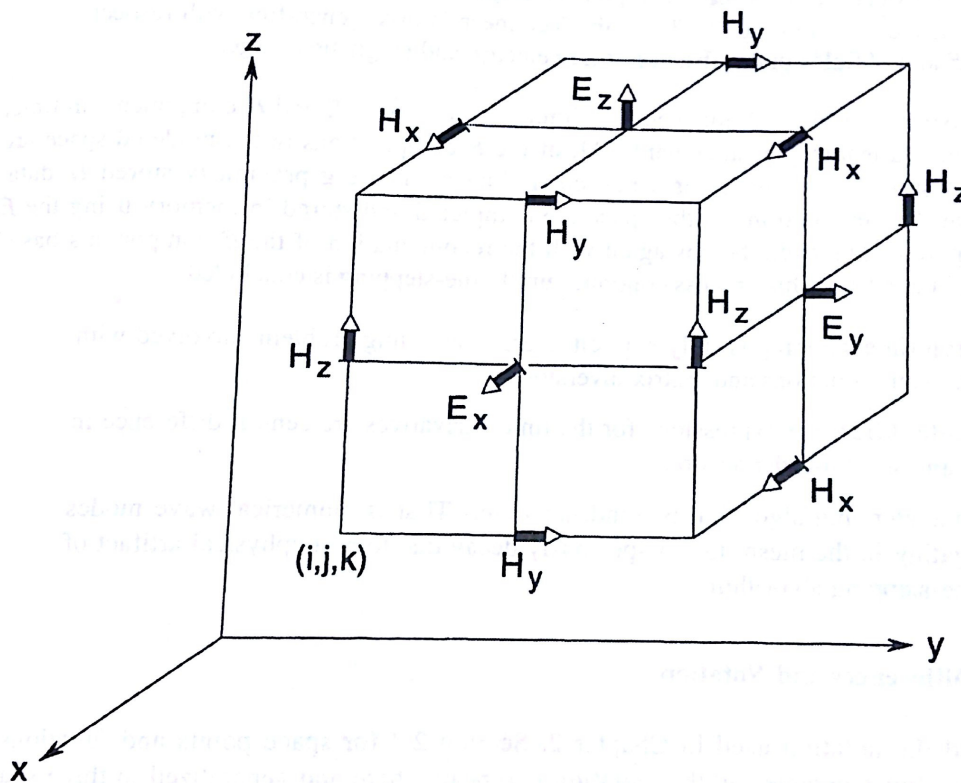
Figure 5: A Yee Cell [1]

Starting with Ampere's law:

$$\frac{\partial E}{\partial t} = \frac{-1}{\varepsilon} \Delta \times H$$

For this example, a loss-less medium with no sources is assumed. The next step is to separate the

vector into components and apply central differencing to these derivatives. The way central differencing works for second order accurate systems is to take the average of position vectors over a length [1]. So, the central differencing of a vector r(x):

$$\frac{\partial r(x)}{\partial x} \approx \frac{r(x+1/2)-r(x-1/2)}{\Delta x}$$

So, the derivative in the x direction of a vector can be approximated as the value of the r vector a half step before minus a half step after divided by the spacing Δx between the points. Remember, it is a time-domain method so it would be evaluated at one time step n. Since the spacing Δx can be an arbitrary spacing, the model detail can be chosen if small structures need to be simulated.

The same kind of differencing can be applied to time derivatives as well:

$$\frac{\partial r(x,t)}{\partial t} \approx \frac{r_x^{n+1/2}-r_x^{n-1/2}}{\Delta t}$$

Where n is the time step and can only take integer values. As in the previous equation, Δt is the size of the difference in times averaged over. Or, in simpler language, it is how long each time step n is. This value can be chosen to evaluate events that are very short duration or events that are long duration.

This method of discretizing derivatives gives great flexibility over how structures are modeled. Choosing a large Δt and Δx can make a model much easier to execute on slower machines. However, the same code can be easily ported to more powerful computers. Changing the values of Δt and Δx will increase the detail of the model and computation time making it easy to scale code to the available hardware.

Now, applying these averaging schemes to Ampere's law, a discretized form can be obtained. For this example, only the x direction will be observed, but it is simple to apply the same method to the other components of E. Writing E in the x direction:

$$\frac{\partial E_x}{\partial t} = \frac{-1}{\varepsilon}\left[\frac{\partial H_z}{\partial y} - \frac{\partial H_y}{\partial z}\right]$$

Now, applying the central differencing method:

11

$$\frac{E_x^{n+1/2} - E_x^{n-1/2}}{\Delta t} = \frac{-1}{\varepsilon} \left[\frac{H_z(j+1/2) - H_z(j-1/2)}{\Delta y} - \frac{H_y(k+1/2) - H_y(k-1/2)}{\Delta z} \right]$$

Where each of these points is assumed to be at a point (i,j,k,n) unless otherwise noted. So the E field is being evaluated at a point E(i,j,k) and the H field at points offset ½ around it.

Rearranging this equation to get the E_x(i,j,k,n+1/2) term alone on one side defines the update scheme. The n+1/2 term is the next value of E in the simulation. This value can be calculated by looking at the current values of H around the E point and the previous value of E at the same point where the previous value of E here would be the Ex(n-1/2) term.

A similar process can be followed to find the other components of E and to find an updating scheme for the H field as well. These steps will not be covered here but can be seen in [1] if the reader desires.

Typically, all of the denominators are eliminated by multiplying all terms by εΔtΔyΔz. These values are all constants and known at the start of the simulation. These terms are all combined into one constant term that is solved for at the beginning of the simulation for efficiency purposes. This gives us a final update equation of:

$$E_x^{n+1/2} = C_a E_x^{n-1/2} + C_b [H_z(j+1/2) + H_z(j-1/2) + H_y(k+1/2) + H_y(k-1/2)]$$

2.2   Cold Plasma

There are several ways to obtain equations for the current density in the presence of a magnetic field. Cummer used [15] as a starting point for his derivation in [4]. This paper will use [11] to derive the equations. While the two sources are equivalent, Booker's derivation is simpler to follow.

The equation for the drift velocity of each species (electrons, positive ions, and negative ions) with collisions as given in [11] is

$$N_l m_l \frac{\partial \vec{v}_l}{\partial t} = N_l q_l (\vec{E} + \vec{v}_l \times \vec{B}_0) - N_l m_l v_l \vec{v}_l$$

Where N_l is the number of particles for a particular species l, m_l is the mass of the particles, q_l is the

charge of the particles, E is the electric field in the plasma, B_0 is the Earth's magnetic field, v_l is the drift velocity, and υ_l is the collision frequency for the species. Next, the current density, J, is added into the equation rather than using the number of particles. This will relate the current density of each species to the electric field and the imposed magnetic field.

$$\vec{J}_l = N_l q_l \vec{v}_l$$

$$\frac{m_l}{q_l}\frac{\partial \vec{J}_l}{\partial t} + \frac{m_l \upsilon_l}{q_l}\vec{J}_l = N_l q_l \vec{E} + N_l q_l (\vec{v}_l \times \vec{B}_0)$$

Here the equation has been rearranged, current density for the species has been substituted, and the parentheses expanded to separate the E from the cross product. Next, the algebraic properties of the cross product can be used to combine more terms while simultaneously multiplying by the charge over the mass.

$$\frac{\partial \vec{J}_l}{\partial t} + \upsilon_l \vec{J}_l = \frac{N_l q_l^2}{m_l}\vec{E} + (N_l q_l \vec{v}_l) \times (\frac{q_l}{m_l}\vec{B}_0)$$

For ω_{pl} and ω_{pl} the above equation can be reduced to the following:

$$\omega_{p_l}^2 = \frac{N_l q_l^2}{\varepsilon_0 m_l} \qquad \vec{\omega}_{c_l} = \frac{q_l \vec{B}_0}{m_l}$$

$$\frac{\partial \vec{J}_l}{\partial t} + \upsilon_l \vec{J}_l = \varepsilon_0 \omega_{p_l}^2 \vec{E} + (\vec{J}_l) \times (\vec{\omega}_{c_l})$$

In this equation, ω_c is the cyclotron frequency and ω_{pl} is the plasma frequency of the species. Using another property of the cross product, the terms can be rearranged. A negative sign can then be factored out from the charge of the cyclotron frequency for the electron and negative ion cases. Since the positive ions have a positive charge, there is a sign difference between the drift velocity for the positive ion and negative ions. Thus, the final equations are the following:

$$\frac{\partial (\vec{J})_e}{\partial t} + v_e (\vec{J})_e = \varepsilon_0 \omega_{p_e}^2 (\vec{E}) + (\vec{\omega})_{c_e} \times (\vec{J})_e$$

13

$$\frac{\partial(\vec{J})_p}{\partial t} + v_p(\vec{J})_p = \varepsilon_0 \omega_{p_p}^2(\vec{E}) - (\vec{\omega})_{c_p} \times (\vec{J})_p$$

$$\frac{\partial(\vec{J})_n}{\partial t} + v_n(\vec{J})_n = \varepsilon_0 \omega_{p_n}^2(\vec{E}) + (\vec{\omega})_{c_n} \times (\vec{J})_n$$

This result also matches the equations that Cummer used in [4].

2.3   History of Cold Plasma in Rectangular Coordinates

The steps used previously to derive the FDTD algorithms can be used to derive a similar result with the new current density equations. This has been done in [10]. Yu's method will be briefly summarized. His motivation for modeling the Ionosphere is broadband analysis of signal propagation through the medium.

First, Yu starts by modeling the Ionosphere as a magnetized cold plasma or anisotropic cold plasma. The governing equations are derived from Maxwell's equations and the Lorentz equation derived previously. The process begins with the following equations [10][11]:

$$\Delta \times (\vec{E}) = -\mu_0 \frac{\partial(\vec{H})}{\partial t} \qquad (1)$$

$$\Delta \times (\vec{H}) = -\varepsilon_0 \frac{\partial(\vec{E})}{\partial t} + (\vec{J})_i + (\vec{J})_s \qquad (2)$$

$$\frac{\partial(\vec{J})_e}{\partial t} + v_e(\vec{J})_e = \varepsilon_0 \omega_{p_e}^2(\vec{E}) + (\vec{\omega})_{c_e} \times (\vec{J})_e \qquad (3)$$

$$\frac{\partial(\vec{J})_p}{\partial t} + v_p(\vec{J})_p = \varepsilon_0 \omega_{p_p}^2(\vec{E}) - (\vec{\omega})_{c_p} \times (\vec{J})_p \qquad (4)$$

$$\frac{\partial(\vec{J})_n}{\partial t} + v_n(\vec{J})_n = \varepsilon_0 \omega_{p_n}^2(\vec{E}) + (\vec{\omega})_{c_n} \times (\vec{J})_n \qquad (5)$$

$$(\vec{J})_I = \sum_l (\vec{J})_l = (\vec{J})_e + (\vec{J})_p + (\vec{J})_n \qquad (6)$$

These equations describe a plasma with collision frequencies v, cyclotron frequencies ω_c, and current

densities J. The subscripts denote different particles within the plasma: e for electrons, p for positive ions, and n for negative ions. J_s is the source current density.

Applying the FDTD derivation to these equations is fairly straightforward. Equations 1 and 2 are very similar to the previous derivation so they will not be covered here. However, equation 3, 4, and 5 are quite different. In particular, the cross product complicates matters somewhat. All three equations are very similar and only equation 3 will be analyzed but the same process can be applied to equations 4 and 5 as well.

First, the vectors are separated into their x, y, and z components. This makes evaluating the cross product much easier. It is important to remember that by separating out each equation, equations 3, 4, and 5 become nine equations. The x component of equation 3 will be analyzed further:

$$\frac{\partial J_{ex}}{\partial t} + v_e J_{ex} = \varepsilon_0 \omega_{p_e}^2 E_x + \omega_{c_{ey}} J_{ez} - \omega_{c_{ez}} J_{ey}$$

Now, central differencing is applied to the time derivative and the J and E values are averaged over a point at time step n+1/2:

$$\frac{J_{ex}^{n+1} - J_{ex}^n}{\Delta t} + v_e \frac{J_{ex}^{n+1} + J_{ex}^n}{2} =$$

$$\varepsilon_0 \omega_{p_e}^2 \frac{E_x^{n+1} + E_x^n}{2} + \omega_{c_{ey}} \frac{J_{ez}^{n+1} + J_{ez}^n}{2} - \omega_{c_{ez}} \frac{J_{ey}^{n+1} + J_{ey}^n}{2}$$

This equation uses the semi-implicit approximation to average J_s and E over a time step. These are the terms that are divided by 2. This equation now looks similar to the previous FDTD equations. The next step is to separate the n+1 terms from the n terms and apply scaling. This will produce a system of equations that can be used to define the updating coefficients. Applying this to each of the x, y, z components of Ampere's law, the following equations are obtained:

$$E_x\big|_{i+1/2,j,k}^{n+1} + \frac{1}{2} J_{ex}\big|_{i+1/2,j,k}^{n+1} + \frac{1}{2} J_{px}\big|_{i+1/2,j,k}^{n+1} + \frac{1}{2} J_{nx}\big|_{i+1/2,j,k}^{n+1} = E_x\big|_{i+1/2,j,k}^{n} - \frac{1}{2} J_{ex}\big|_{i+1/2,j,k}^{n} -$$

$$\frac{1}{2} J_{px}\big|_{i+1/2,j,k}^{n} - \frac{1}{2} J_{nx}\big|_{i+1/2,j,k}^{n} + \frac{(\Delta t)^2}{\varepsilon_0 \mu_0 \Delta y}\left(\frac{\Delta H_z}{\Delta y}\right)_{i+1/2,j,k}^{n+1/2} - \frac{(\Delta t)^2}{\varepsilon_0 \mu_0 \Delta z}\left(\frac{\Delta H_y}{\Delta z}\right)_{i+1/2,j,k}^{n+1/2} - J_{Sx}\big|_{i+1/2,j,k}^{n+1/2}$$

$$E_y\Big|_{i+1/2,j,k}^{n+1}+\frac{1}{2}J_{ey}\Big|_{i+1/2,j,k}^{n+1}+\frac{1}{2}J_{py}\Big|_{i+1/2,j,k}^{n+1}+\frac{1}{2}J_{ny}\Big|_{i+1/2,j,k}^{n+1}=E_y\Big|_{i+1/2,j,k}^{n}-\frac{1}{2}J_{ey}\Big|_{i+1/2,j,k}^{n}-$$

$$\frac{1}{2}J_{py}\Big|_{i+1/2,j,k}^{n}-\frac{1}{2}J_{ny}\Big|_{i+1/2,j,k}^{n}+\frac{(\Delta t)^2}{\varepsilon_0\mu_0\Delta z}\Big(\frac{\Delta H_x}{\Delta z}\Big)_{i+1/2,j,k}^{n+1/2}-\frac{(\Delta t)^2}{\varepsilon_0\mu_0\Delta x}\Big(\frac{\Delta H_z}{\Delta x}\Big)_{i+1/2,j,k}^{n+1/2}-J_{Sy}\Big|_{i+1/2,j,k}^{n+1/2}$$

$$E_z\Big|_{i+1/2,j,k}^{n+1}+\frac{1}{2}J_{ez}\Big|_{i+1/2,j,k}^{n+1}+\frac{1}{2}J_{pz}\Big|_{i+1/2,j,k}^{n+1}+\frac{1}{2}J_{nz}\Big|_{i+1/2,j,k}^{n+1}=E_z\Big|_{i+1/2,j,k}^{n}-\frac{1}{2}J_{ez}\Big|_{i+1/2,j,k}^{n}-$$

$$\frac{1}{2}J_{pz}\Big|_{i+1/2,j,k}^{n}-\frac{1}{2}J_{nz}\Big|_{i+1/2,j,k}^{n}+\frac{(\Delta t)^2}{\varepsilon_0\mu_0\Delta x}\Big(\frac{\Delta H_y}{\Delta x}\Big)_{i+1/2,j,k}^{n+1/2}-\frac{(\Delta t)^2}{\varepsilon_0\mu_0\Delta y}\Big(\frac{\Delta H_x}{\Delta y}\Big)_{i+1/2,j,k}^{n+1/2}-J_{Sz}\Big|_{i+1/2,j,k}^{n+1/2}$$

This completes the derivation for equation 3. The same steps can be taken to derive similar results for equations 4 and 5. To obtain better stability and accuracy, Yu scaled the H and J components [10]. For the x component of equation 3, this gives a final result of:

$$\frac{-(\omega_{p_e}\Delta t)^2}{2}E_x\Big|_{i+1/2,j,k}^{n+1}+\Big(1+\frac{v_e\Delta t}{2}\Big)J_{ex}\Big|_{i+1/2,j,k}^{n+1}\frac{\omega_{c_{ez}}\Delta t}{2}J_{ey}\Big|_{i+1/2,j,k}^{n+1}\frac{\omega_{c_{ey}}\Delta t}{2}J_{ez}\Big|_{i+1/2,j,k}^{n+1}=$$

$$\frac{(\omega_{p_e}\Delta t)^2}{2}E_x\Big|_{i+1/2,j,k}^{n}+\Big(1+\frac{v_e\Delta t}{2}\Big)J_{ex}\Big|_{i+1/2,j,k}^{n}\frac{\omega_{c_{ez}}\Delta t}{2}J_{ey}\Big|_{i+1/2,j,k}^{n+1}\frac{\omega_{c_{ey}}\Delta t}{2}J_{ez}\Big|_{i+1/2,j,k}^{n}$$

This produces 12 equations: 3 for equations 2, 3, 4, and 5 each. By combining these discritized equations with the standard equations for a discritized Faraday's Law gives us a system of 12 unknowns and 12 equations. Solving this system is most easily accomplished by using matrices. A, B, and C matrices are defined for the n+1, n, and n+1/2 term respectively:

$$[A] \cdot \begin{bmatrix} E_x\big|_{i+1/2,j,k}^{n+1} \\ E_y\big|_{i+1/2,j,k}^{n+1} \\ E_z\big|_{i+1/2,j,k}^{n+1} \\ J_{ex}\big|_{i+1/2,j,k}^{n+1} \\ J_{px}\big|_{i+1/2,j,k}^{n+1} \\ J_{nx}\big|_{i+1/2,j,k}^{n+1} \\ J_{ey}\big|_{i+1/2,j,k}^{n+1} \\ J_{py}\big|_{i+1/2,j,k}^{n+1} \\ J_{ny}\big|_{i+1/2,j,k}^{n+1} \\ J_{ez}\big|_{i+1/2,j,k}^{n+1} \\ J_{pz}\big|_{i+1/2,j,k}^{n+1} \\ J_{nz}\big|_{i+1/2,j,k}^{n+1} \end{bmatrix} = [B] \cdot \begin{bmatrix} E_x\big|_{i+1/2,j,k}^{n} \\ E_y\big|_{i+1/2,j,k}^{n} \\ E_z\big|_{i+1/2,j,k}^{n} \\ J_{ex}\big|_{i+1/2,j,k}^{n} \\ J_{px}\big|_{i+1/2,j,k}^{n} \\ J_{nx}\big|_{i+1/2,j,k}^{n} \\ J_{ey}\big|_{i+1/2,j,k}^{n} \\ J_{py}\big|_{i+1/2,j,k}^{n} \\ J_{ny}\big|_{i+1/2,j,k}^{n} \\ J_{ez}\big|_{i+1/2,j,k}^{n} \\ J_{pz}\big|_{i+1/2,j,k}^{n} \\ J_{nz}\big|_{i+1/2,j,k}^{n} \end{bmatrix} + [C] \begin{bmatrix} \left(\dfrac{\Delta H_z}{\Delta y}\right)_{i+1/2,j,k}^{n+1/2} \\ \left(\dfrac{\Delta H_y}{\Delta z}\right)_{i+1/2,j,k}^{n+1/2} \\ \left(\dfrac{\Delta H_x}{\Delta z}\right)_{i+1/2,j,k}^{n+1/2} \\ \left(\dfrac{\Delta H_z}{\Delta x}\right)_{i+1/2,j,k}^{n+1/2} \\ \left(\dfrac{\Delta H_y}{\Delta x}\right)_{i+1/2,j,k}^{n+1/2} \\ \left(\dfrac{\Delta H_x}{\Delta y}\right)_{i+1/2,j,k}^{n+1/2} \\ J_{Sx}\big|_{i+1/2,j,k}^{n+1/2} \\ J_{Sy}\big|_{i+1/2,j,k}^{n+1/2} \\ J_{Sz}\big|_{i+1/2,j,k}^{n+1/2} \end{bmatrix}$$

By moving the A matrix over, an equation relating the n +1 terms to the known n and n +1/2 terms is produced. All values in the A, B, and C matrices are known as well. This produces an updating equation for each of the n+1 terms to be solved at every time step. This largely completes the model, with the exception of some cell averaging. The cell averaging is required to find components that do not exist directly at a grid location. This is done by averaging the diagonal corners of the non-existent cell, or the cells half a step in each direction. This gives us a final result of:

$$
\begin{vmatrix}
E_x|_{i+1/2,j,k}^{n+1} \\
E_y|_{i,j+1/2,k}^{n+1} \\
E_z|_{i,j,k+1/2}^{n+1} \\
J_{ex}|_{i+1/2,j,k}^{n+1} \\
J_{px}|_{i+1/2,j,k}^{n+1} \\
J_{nx}|_{i+1/2,j,k}^{n+1} \\
J_{ey}|_{i,j+1/2,k}^{n+1} \\
J_{py}|_{i,j+1/2,k}^{n+1} \\
J_{ny}|_{i,j+1/2,k}^{n+1} \\
J_{ez}|_{i,j,k+1/2}^{n+1} \\
J_{pz}|_{i,j,k+1/2}^{n+1} \\
J_{nz}|_{i,j,k+1/2}^{n+1}
\end{vmatrix}
= [A^{-1}B] \cdot
\begin{vmatrix}
E_x^n \\
E_y^n \\
E_z^n \\
J_{ex}^n \\
J_{px}^n \\
J_{nx}^n \\
J_{ey}^n \\
J_{py}^n \\
J_{ny}^n \\
J_{ez}^n \\
J_{pz}^n \\
J_{nz}^n
\end{vmatrix}
+ [A^{-1}C]
\begin{vmatrix}
(\dfrac{\Delta H_z}{\Delta y})^{n+1/2} \\
(\dfrac{\Delta H_y}{\Delta z})^{n+1/2} \\
(\dfrac{\Delta H_x}{\Delta z})^{n+1/2} \\
(\dfrac{\Delta H_z}{\Delta x})^{n+1/2} \\
(\dfrac{\Delta H_y}{\Delta x})^{n+1/2} \\
(\dfrac{\Delta H_x}{\Delta y})^{n+1/2} \\
J_{Sx}^{n+1/2} \\
J_{Sy}^{n+1/2} \\
J_{Sz}^{n+1/2}
\end{vmatrix}
$$

$$
[C]=
\begin{vmatrix}
\dfrac{dt^2}{\varepsilon_0\mu_0 dz} & -\dfrac{dt^2}{\varepsilon_0\mu_0 dy} & 0 & 0 & 0 & 0 & -1 & 0 & 0 \\
0 & 0 & \dfrac{dt^2}{\varepsilon_0\mu_0 dx} & \dfrac{dt^2}{\varepsilon_0\mu_0 dz} & 0 & 0 & 0 & -1 & 0 \\
0 & 0 & 0 & 0 & \dfrac{dt^2}{\varepsilon_0\mu_0 dy} & \dfrac{dt^2}{\varepsilon_0\mu_0 dx} & 0 & 0 & -1 \\
0 & 0 & 0 & 0 & 0 & 0 & 0 & 0 & 0 \\
0 & 0 & 0 & 0 & 0 & 0 & 0 & 0 & 0 \\
0 & 0 & 0 & 0 & 0 & 0 & 0 & 0 & 0 \\
0 & 0 & 0 & 0 & 0 & 0 & 0 & 0 & 0 \\
0 & 0 & 0 & 0 & 0 & 0 & 0 & 0 & 0 \\
0 & 0 & 0 & 0 & 0 & 0 & 0 & 0 & 0 \\
0 & 0 & 0 & 0 & 0 & 0 & 0 & 0 & 0 \\
0 & 0 & 0 & 0 & 0 & 0 & 0 & 0 & 0 \\
0 & 0 & 0 & 0 & 0 & 0 & 0 & 0 & 0
\end{vmatrix}
$$

$$[A]=\begin{bmatrix}
1 & 0 & 0 & .5 & .5 & .5 & 0 & 0 & 0 & 0 & 0 & 0 \\
0 & 1 & 0 & 0 & 0 & 0 & .5 & .5 & .5 & 0 & 0 & 0 \\
0 & 0 & 1 & 0 & 0 & 0 & 0 & 0 & 0 & .5 & .5 & .5 \\
-\dfrac{(\omega_{P_e}dt)^2}{2} & 0 & 0 & 1+\dfrac{v_e dt}{2} & 0 & 0 & \dfrac{\omega_{Cez}dt}{2} & 0 & 0 & -\dfrac{\omega_{Cey}dt}{2} & 0 & 0 \\
-\dfrac{(\omega_{P_p}dt)^2}{2} & 0 & 0 & 0 & 1+\dfrac{v_p dt}{2} & 0 & 0 & \dfrac{\omega_{Cpz}dt}{2} & 0 & 0 & -\dfrac{\omega_{Cpy}dt}{2} & 0 \\
-\dfrac{(\omega_{P_n}dt)^2}{2} & 0 & 0 & 0 & 0 & 1+\dfrac{v_n dt}{2} & 0 & 0 & \dfrac{\omega_{Cnz}dt}{2} & 0 & 0 & -\dfrac{\omega_{Cny}dt}{2} \\
0 & -\dfrac{(\omega_{P_e}dt)^2}{2} & 0 & -\dfrac{\omega_{Cez}dt}{2} & 0 & 0 & 1+\dfrac{v_e dt}{2} & 0 & 0 & \dfrac{\omega_{Cex}dt}{2} & 0 & 0 \\
0 & -\dfrac{(\omega_{P_p}dt)^2}{2} & 0 & 0 & -\dfrac{\omega_{Cpz}dt}{2} & 0 & 0 & 1+\dfrac{v_p dt}{2} & 0 & 0 & \dfrac{\omega_{Cpx}dt}{2} & 0 \\
0 & -\dfrac{(\omega_{P_n}dt)^2}{2} & 0 & 0 & 0 & -\dfrac{\omega_{Cnz}dt}{2} & 0 & 0 & 1+\dfrac{v_n dt}{2} & 0 & 0 & \dfrac{\omega_{Cnx}dt}{2} \\
0 & 0 & -\dfrac{(\omega_{P_e}dt)^2}{2} & -\dfrac{\omega_{Cey}dt}{2} & 0 & 0 & \dfrac{\omega_{Cex}dt}{2} & 0 & 0 & 1+\dfrac{v_e dt}{2} & 0 & 0 \\
0 & 0 & -\dfrac{(\omega_{P_p}dt)^2}{2} & 0 & -\dfrac{\omega_{Cpy}dt}{2} & 0 & 0 & \dfrac{\omega_{Cpx}dt}{2} & 0 & 0 & 1+\dfrac{v_p dt}{2} & 0 \\
0 & 0 & -\dfrac{(\omega_{P_n}dt)^2}{2} & 0 & 0 & -\dfrac{\omega_{Cny}dt}{2} & 0 & 0 & \dfrac{\omega_{Cnx}dt}{2} & 0 & 0 & 1+\dfrac{v_n dt}{2}
\end{bmatrix}$$

$$[B]=\begin{vmatrix}
1 & 0 & 0 & -.5 & -.5 & -.5 & 0 & 0 & 0 & 0 & 0 & 0 \\
0 & 1 & 0 & 0 & 0 & 0 & -.5 & -.5 & -.5 & 0 & 0 & 0 \\
0 & 0 & 1 & 0 & 0 & 0 & 0 & 0 & 0 & -.5 & -.5 & -.5 \\
\dfrac{(\omega_{P_e} dt)^2}{2} & 0 & 0 & 1-\dfrac{v_e\,dt}{2} & 0 & 0 & -\dfrac{\omega_{Cez}\,dt}{2} & 0 & 0 & \dfrac{\omega_{Cey}\,dt}{2} & 0 & 0 \\
\dfrac{(\omega_{P_p} dt)^2}{2} & 0 & 0 & 0 & 1-\dfrac{v_p\,dt}{2} & 0 & 0 & \dfrac{\omega_{Cpz}\,dt}{2} & 0 & 0 & -\dfrac{\omega_{Cpy}\,dt}{2} & 0 \\
\dfrac{(\omega_{P_n} dt)^2}{2} & 0 & 0 & 0 & 0 & 1-\dfrac{v_n\,dt}{2} & 0 & 0 & -\dfrac{\omega_{Cnz}\,dt}{2} & 0 & 0 & \dfrac{\omega_{Cny}\,dt}{2} \\
0 & \dfrac{(\omega_{P_e} dt)^2}{2} & 0 & \dfrac{\omega_{Cez}\,dt}{2} & 0 & 0 & 1-\dfrac{v_e\,dt}{2} & 0 & 0 & -\dfrac{\omega_{Cex}\,dt}{2} & 0 & 0 \\
0 & \dfrac{(\omega_{P_p} dt)^2}{2} & 0 & 0 & -\dfrac{\omega_{Cpz}\,dt}{2} & 0 & 0 & 1-\dfrac{v_p\,dt}{2} & 0 & 0 & \dfrac{\omega_{Cpx}\,dt}{2} & 0 \\
0 & \dfrac{(\omega_{P_n} dt)^2}{2} & 0 & 0 & 0 & \dfrac{\omega_{Cnz}\,dt}{2} & 0 & 0 & 1-\dfrac{v_n\,dt}{2} & 0 & 0 & -\dfrac{\omega_{Cnx}\,dt}{2} \\
0 & 0 & \dfrac{(\omega_{P_e} dt)^2}{2} & -\dfrac{\omega_{Cey}\,dt}{2} & 0 & 0 & \dfrac{\omega_{Cex}\,dt}{2} & 0 & 0 & 1-\dfrac{v_e\,dt}{2} & 0 & 0 \\
0 & 0 & \dfrac{(\omega_{P_p} dt)^2}{2} & 0 & \dfrac{\omega_{Cpy}\,dt}{2} & 0 & 0 & -\dfrac{\omega_{Cpx}\,dt}{2} & 0 & 0 & 1-\dfrac{v_p\,dt}{2} & 0 \\
0 & 0 & \dfrac{(\omega_{P_n} dt)^2}{2} & 0 & 0 & -\dfrac{\omega_{Cny}\,dt}{2} & 0 & 0 & \dfrac{\omega_{Cnx}\,dt}{2} & 0 & 0 & 1-\dfrac{v_n\,dt}{2}
\end{vmatrix}$$

Chapter 3

Derivation of the Geodesic Grid Cold Plasma Updates

3.1   Geodesic Grid Formulation

The geodesic grid was chosen because of its use in other papers [12]. First, it has been used in the past to apply FDTD to an ELF/ULF propagation problem. In that implementation, it was accurate to within ± 0.5 dB/Mm [12] and was able to run on a standard desktop computer rather than a supercomputer. While the geodesic grid requires more memory then the Latitude-Longitude grid, the reduction in processing time is desirable [12].

The first step is to visualize what the grid will look like. It is most comparable to a soccer ball, a series of hexagons covering a sphere. However, hexagons alone cannot be used to cover a sphere and a minimum of 12 pentagons must be used as well.

These hexagons and pentagons will be the individual cells of the FDTD grid as seen in Figure 4. The pentagons are the points where the larger triangles meet. Previously, the Yee cell was used for each cell. However, the Yee cell is only applicable in a rectangular coordinate system and a new set of updating equations will need to be derived. In the interest of brevity, half of the governing equations will be derived. A more complete solution can be found in [12].

The geometry of the geodesic FDTD model requires that the TE and TM modes be solved separately. The TM case will be analyzed first, followed by the TE. After equations have been derived for the separate cases, the equations will be combined to form one large matrix, similar to the Yu's rectangular system. The matrix will then be rearranged to solve for n + 1 terms, producing the updating equations for each time step.

3.2   TM Equations

The derivation begins with Faraday's equation. Rather then using the differential form of the

equation, the integral form is chosen. This is the natural choice for the geometry of the grid:

$$\frac{\partial}{\partial t}\iint_A B \cdot dA = -\oint_L E \cdot dL$$

Starting with the left hand side of the equation, the time averaging used previously is applied to the derivative. The area integral can also be averaged as the field over the area of one cell. A will be used to represent the area of one cell. This results in the following equation:

$$\frac{\partial}{\partial t}\iint_A B \cdot dA = \mu A \frac{H_1^{n+1/2} - H_1^{n-1/2}}{\Delta t}$$

It is important to realize that this area is the area of a square created by the radial E fields adjacent to H_1 and the E fields a half cell above and below it. This information is key to solving the right hand side of the equation:

$$-\oint_L E \cdot dL = -\left(-\Delta r\, E_{r,i-1}^n + \Delta r\, E_r^n - \delta(1)\, E_{1,k+1/2}^n + \delta(1)\, E_{1,k-1/2}^n\right)$$

The Δr term in the previous equation is the space between the geodesic TM grid and the triangular TE grid half a cell above. Combining the two equation together and rearranging, produces an update equation for the H_1 term. It is important to notice that H_1 is divided by the area of the square that it passes through. This can be used to cancel a pair of Δr and $\delta(1)$ terms:

$$H_1^{n+3/2} = H_1^{n+1/2} + \frac{\Delta t}{\mu\delta(1)}\left(E_{r,i-1}^{n+1} - E_r^{n+1}\right) + \frac{\Delta t}{\mu\Delta r}\left(E_{1,k+1/2}^{n+1} + E_{1,k-1/2}^{n+1}\right)$$

Applying this concept to the other H vectors, produces the following equations:

$$H_2^{n+3/2} = H_2^{n+1/2} + \frac{\Delta t}{\mu\delta(2)}\left(E_{r,i-1,j-1}^{n+1} - E_r^{n+1}\right) + \frac{\Delta t}{\mu\Delta r}\left(E_{2,k+1/2}^{n+1} + E_{2,k-1/2}^{n+1}\right)$$

$$H_3^{n+3/2} = H_1^{n+1/2} + \frac{\Delta t}{\mu\delta(3)}\left(E_{r,j-1}^{n+1} - E_r^{n+1}\right) + \frac{\Delta t}{\mu\Delta r}\left(E_{3,k+1/2}^{n+1} - E_{3,k-1/2}^{n+1}\right)$$

Next, the same process is applied to Ampere's law. Again, the integral form is more convenient for this geometry rather than the differential form used in rectangular coordinates:

22

$$\frac{\partial}{\partial t}\iint_A D \cdot dA = \oint_L H \cdot dL - \iint_A J_s \cdot dA - \iint_A J_I \cdot dA$$

Now, the magnetic fields are defined as circling the electric field along the edge of a hexagon. Electric field is also defined as coming out of the center of the hexagon as seen in Figure 6. The line integral of H can now be evaluated.
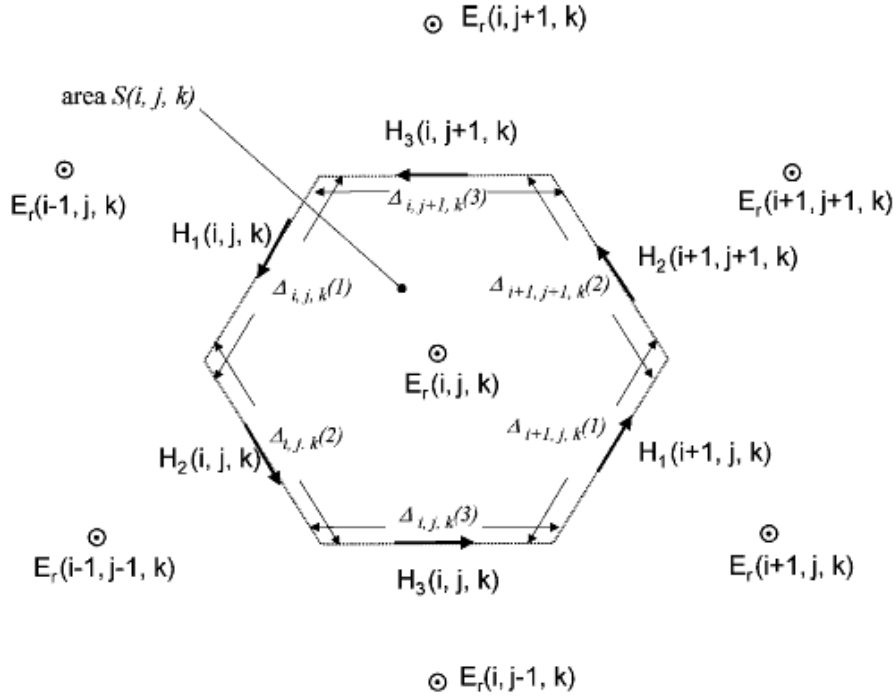
Figure 6: A Single Geodesic Cell for TM Modes [12]

$$\oint_L H \cdot dL = H_1 \Delta(1) + H_2 \Delta(2) + H_3 \Delta(3) - H_1 \Delta_{i+1}(1) - H_2 \Delta_{i+1,j+1}(2) - H_3 \Delta_{j+1}(3)$$

The left hand side of Ampere's law also needs to be analyzed. The central differencing used previously can be applied here as well. S will be used to denote the area of a hexagon.

$$\frac{\partial}{\partial t}\iint_A D \cdot dA = \varepsilon S \left(\frac{E^{n+1} - E^n}{\Delta t}\right)$$

By symmetry, it is apparent thay the current density J will produce a similar result:

$$\frac{\partial}{\partial t} \iint_A J_{Ir} \cdot dA = S\left(\frac{J_{Ir}^{n+1} - J_{Ir}^n}{\Delta t}\right)$$

Combining all of these equations, a single equation to calculate the next value of the electric field is obtained.

$$E_r^{n+1} + \frac{J_{Ir}^{n+1}}{2} = E_r^n + \frac{\Delta t}{\varepsilon S}\left(H_1 \Delta(1) + H_2 \Delta(2) + H_3 \Delta(3) - H_1 \Delta_{i+1}(1) - H_2 \Delta_{i+1, j+1}(2) - H_3 \Delta_{j+1}(3)\right)$$

$$- \frac{\Delta t}{2\varepsilon} J_{Ir}^n + \frac{\Delta t}{\varepsilon} J_{Sr}^{n+1/2}$$

It is very important to remember that J_{Ir} is not just one current density, but the sum of all the radial current densities for the plasma.

Next, equations 3, 4, and 5, the equations relating the current density of the plasma and the electric field will be analyzed. However, these equations cannot be discretizied in the same manner as in the rectangular derivation. The issue is the cross product. Previously, Yu separated the cross product by converting the vectors into their x, y, and z components. However, these components are not defined in the geodesic grid. Instead, some substitutions will need to be made. First, the cyclotron frequency will be replaced:

$$\omega_{cl} = \frac{q_l(\vec{B})}{m_l}$$

This relates the cyclotron frequency to the charge and mass of the medium as well as the Earth's global magnetic field. Using this and a different form of the cross product, the following is obtained:

$$\frac{\partial(\vec{J})_e}{\partial t} + v_e(\vec{J})_e = \varepsilon_0 \omega_{p_e}^2 (\vec{E}) + \left|\frac{q_e B}{m_e}\right| |J_e| \sin(\theta)$$

This θ is the angle between the Earth's magnetic field and the direction of the current density. While the Earth's magnetic field varies with time, it varies slowly compared to the scale used. As such, it can be treated as a fixed vector. Since the current density is also fixed for each cell, this angle does not vary

with time, only location. This makes discretizing the equation much easier:

$$\frac{J_{e_r}^{n+1}-J_{e_r}^n}{\Delta t}+v_e\frac{J_{e_r}^{n+1}+J_{e_r}^n}{2}=\varepsilon_0\omega_{p_e}^2\frac{E_r^{n+1}+E_r^n}{2}-|\frac{q_eB}{m_e}||\frac{J_{e_r}^{n+1}+J_{e_r}^n}{2}|\sin(\theta)$$

Previously, equations were rearranged to get all of the n + 1 terms on one side with the n terms on the other side. However, this equation has an n + 1 and n term locked into an absolute value. There is no mathematical way to separate these terms. To approach this problem, it is beneficial to consider the following cases:

$$|J_{e_r}^{n+1}+J_{e_r}^n|=|J_{e_r}^{n+1}|+|J_{e_r}^n|\mathit{iff}\,J_{e_r}>0 \qquad |(-J_{e_r}^{n+1})+0|=|(-J_{e_r}^{n+1})|+|0|$$

$$|(-J_{e_r}^{n+1})+(-J_{e_r}^n)|=|(-J_{e_r}^{n+1})|+|(-J_{e_r}^n)| \qquad |J_{e_r}^{n+1}+(-J_{e_r}^n)|\neq|J_{e_r}^{n+1}|+|-J_{e_r}^n|$$

By observation, if the current value of J is of the same sign as the previous value, regardless if they are positive or negative, then the absolute value can be separated. Also, as long as one of the J terms is zero, the absolute value can still be separated. The only concern is when the current value is of a different sign then the previous. However, in the FDTD updating scheme, the current value will not change suddenly from the previous, it will always slowly approach zero before switching. While the current value will not necessarily equal zero, when it shifts from positive to negative, the previous value should be quite small. The error introduced by this estimation is negligible. Using this information, our current density equation can be rearranged to separate the n + 1 terms from the n terms:

$$J_{e_r}^{n+1}+\frac{\Delta t\,v_e}{2}J_{e_r}^{n+1}-\frac{\Delta t\varepsilon_0\omega_{p_e}^2}{2}E_r^{n+1}+|\frac{q_eB}{m_e}|\frac{\Delta t\sin(\theta)}{2}|J_{e_r}^{n+1}|=J_{e_r}^n-\frac{\Delta t\,v_e}{2}J_{e_r}^n+$$

$$\frac{\Delta t\varepsilon_0\omega_{p_e}^2}{2}E_r^n-|\frac{q_eB}{m_e}|\frac{\Delta t\sin(\theta)}{2}|J_{e_r}^n|$$

The same process can be applied to the other current density equations to obtain similar results. This gives us the final equations for the TM case:

25

$$J_{p_r}^{n+1} + \frac{\Delta t\, v_p}{2} J_{p_r}^{n+1} - \frac{\Delta t \varepsilon_0 \omega_{p_p}^2}{2} E_r^{n+1} + \left|\frac{q_p B}{m_p}\right| \frac{\Delta t \sin(\theta)}{2} |J_{p_r}^{n+1}| = J_{p_r}^n - \frac{\Delta t\, v_p}{2} J_{p_r}^n +$$

$$\frac{\Delta t \varepsilon_0 \omega_{p_p}^2}{2} E_r^n + \left|\frac{q_p B}{m_p}\right| \frac{\Delta t \sin(\theta)}{2} |J_{p_r}^n|$$

$$J_{n_r}^{n+1} + \frac{\Delta t\, v_n}{2} J_{n_r}^{n+1} - \frac{\Delta t \varepsilon_0 \omega_{p_n}^2}{2} E_r^{n+1} + \left|\frac{q_n B}{m_n}\right| \frac{\Delta t \sin(\theta)}{2} |J_{n_r}^{n+1}| = J_{n_r}^n - \frac{\Delta t\, v_n}{2} J_{n_r}^n +$$

$$\frac{\Delta t \varepsilon_0 \omega_{n_l}^2}{2} E_r^n - \left|\frac{q_n B}{m_n}\right| \frac{\Delta t \sin(\theta)}{2} |J_{n_r}^n|$$

This completes the derivation for the TM case. However, this is only half of the equations needed.

3.3   TE Equations

The TE case has a slightly different topology. It can be represented with triangles overlaid onto the hexagon as can be seen in Figure 7. Each triangle's corners align with the grid center of the hexagonal cells above and below it. Note that there are two E_1 and E_3 values, while there remains only one E_2 value in between the two triangles.

Here, the E fields are bisecting the H fields in the geodesic grid half a cell below. The H fields are now on the vertices of the hexagonal cells. These new E fields create triangles around the new H fields. Each pair of triangles becomes a new cell in this grid. The process for deriving the update equations for this grid is very similar to the TM case. Beginning with Faraday's law in integral form:
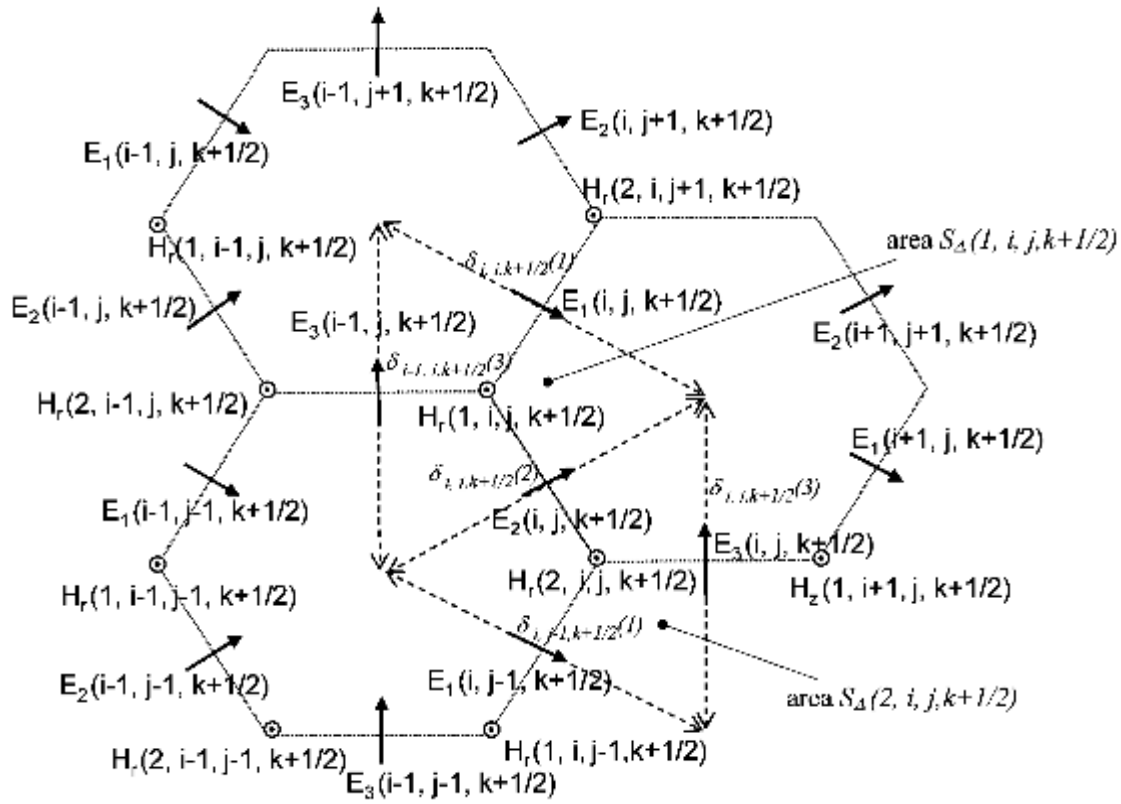
Figure 7: TE Mode Cells Overlaid on Hexagonal Cells [12]

$$\frac{\partial}{\partial t}\iint_A B\cdot dA=-\oint_L E\cdot dL$$

Rather then derive the equation from scratch, a symmetry can be noticed between this equation and Ampere's law but with the B and E fields interchanged and a different field configuration. Noticing this symmetry, the resulting equations should be similar to the TM case. Again, for simplicity, each term of the equation will analyzed separately.

$$\frac{\partial}{\partial t}\iint_A B\cdot dA=\frac{S\mu}{\Delta t}\left(H_r^{n+3/2}(1)-H_r^{n+1/2}(1)\right)$$

$$-\oint_L E\cdot dL=\left(-E_1^n\delta(1)+E_2^n\delta(2)-E_3^n\delta(3)_{i-1}\right)$$

As expected, the equations look similar to the TM case with the exception of the different geometry. In this equation, the δ terms are the lengths of each triangle's sides and the S is the area of

27

one triangle. Re arranging produces an updating equation for $H_r(1)$.

$$H_r^{n+3/2}(1) = H_r^{n+1/2}(1) + \frac{\Delta t}{\mu S}\left(-E_1^n \delta(1) + E_2^n \delta(2) - E_3^n \delta(3)_{i-1}\right)$$

Following the same process, a similar equation for $H_r(2)$ is formed.

$$H_r^{n+3/2}(2) = H_r^{n+1/2}(2) + \frac{\Delta t}{\mu S}\left(E_1^n \delta(1)_{j-1} - E_2^n \delta(2) + E_3^n \delta(3)\right)$$

Next, the same methodology as in the TM case can be applied to the remaining equations. Again, the terms are discritized separately, then combined and rearranged.

$$\frac{\partial}{\partial t} \iint_A D \cdot dA = \frac{\varepsilon_0}{\Delta t} \Delta_{k+1/2}(1) \Delta r \left(E_{1,k+1/2}^{n+1} - E_{1,k+1/2}^n\right)$$

It is important to recognize some of the new values in this equation. While this is an area integral, rather than use a variable to represent the area of one cell, the area has been separated into its components. The area that is being integrated over is the square created by the vertical distance Δr between one set of hexagons and the next, and the horizontal length $\Delta(1)$ between two H_r locations along the side of a hexagonal cell. This will allow more simplification when the equation is rearranged.

$$\oint_L H \cdot dL = -\Delta r\, H_{r,k+1/2}^{n+1/2}(1) + \Delta r\, H_{j+1,k+1/2}^{(n+1/2)}(2) + \Delta_{k+1/2}(1) H_{1,k+1}^{n+1/2} - \Delta_{k+1/2}(1) H_1^{n+1/2}$$

$$-\iint_A J_s \cdot dA = -\Delta_{k+1/2}(1) \Delta r\, J_{s_1}^{n+1/2}$$

$$-\iint_A J_I \cdot dA = \frac{-\Delta_{k+1/2}(1)\Delta r}{2}\left(J_{I_1,k+1/2}^{n+1} + J_{I_1,k+1/2}^n\right)$$

Examining the equations, it can be seen that there are some terms that will cancel when the equation is rearranged. A pair of $\Delta_{k+1/2}(1)$ and Δr terms will cancel from the H terms, simplifying the equation slightly. After combining and simplifying our equation, the remaining terms are:

$$E_{1,k+1/2}^{n+1} + \frac{\Delta t}{2\varepsilon_0} J_{I_1,k+1/2}^{n+1} = E_{1,k+1/2}^n + \frac{\Delta t}{\varepsilon_0}\left(\frac{-J_{I_1,k+1/2}^n}{2} + \frac{H_{r,j+1,k+1/2}^{n+1/2}(2) - H_{r,k+1/2}^{n+1/2}(1)}{\Delta_{k+1/2}(1)} + \frac{H_{1,k+1}^{n+1/2} - H_1^{n+1/2}}{\Delta r}\right)$$

$$-\frac{\Delta t}{\varepsilon_0}J_{s_1,k+1/2}^{n+1/2}$$

Performing the same operation for E_2 and E_3, produces similar equations:

$$E_{2,k+1/2}^{n+1}+\frac{\Delta t}{2\varepsilon_0}J_{I_2,k+1/2}^{n+1}=E_{2,k+1/2}^n-\frac{\Delta t}{\varepsilon_0}\left(\frac{J_{I_2,k+1/2}^n}{2}+\frac{H_{r,k+1/2}^{n+1/2}(2)-H_{r,k+1/2}^{n+1/2}(1)}{\Delta_{k+1/2}(2)}-\frac{H_{2,k+1}^{n+1/2}+H_2^{n+1/2}}{\Delta r}\right)$$

$$-\frac{\Delta t}{\varepsilon_0}J_{s_2,k+1/2}^{n+1/2}$$

$$E_{3,k+1/2}^{n+1}+\frac{\Delta t}{2\varepsilon_0}J_{I_3,k+1/2}^{n+1}=E_{3,k+1/2}^n-\frac{\Delta t}{\varepsilon_0}\left(\frac{J_{I_3,k+1/2}^n}{2}+\frac{H_{r,i+1,j-1,k+1/2}^{n+1/2}(1)-H_{r,k+1/2}^{n+1/2}(2)}{\Delta_{k+1/2}(3)}+\frac{H_3^{n+1/2}-H_{3,k+1}^{n+1/2}}{\Delta r}\right)$$

$$-\frac{\Delta t}{\varepsilon_0}J_{s_3,k+1/2}^{n+1/2}$$

The remaining equations for the TE case are the equations governing the plasma current density. The derivation is similar to the electric field equations since they are collocated. However, there are some differences. As with the TM case, the same substitution for the cyclotron frequency will be used as well as using the alternative form of the cross product. After these substitutions and discretizing the equations produces:

$$\frac{J_{e_1,k+1/2}^{n+1}-J_{e_1,k+1/2}^n}{\Delta t}+v_e\left(\frac{J_{e_1,k+1/2}^{n+1}-J_{e_1,k+1/2}^n}{2}\right)=\varepsilon_0\omega_{p_e}^2\left(\frac{E_{1,k+1/2}^{n+1}+E_{1,k+1/2}^n}{2}\right)+\left|\frac{q_eB}{m_e}\right\|\frac{J_{e_1,k+1/2}^{n+1}-J_{e_1,k+1/2}^n}{2}\left|\sin(\theta)\right.$$

Rearranging this equation and moving all of the n+1 terms to the left and the n terms to the right, leaves:

$$J_{e_1,k+1/2}^{n+1}+\frac{\Delta t v_e}{2}J_{e_1,k+1/2}^{n+1}-\frac{\Delta t\varepsilon_0\omega_{p_e}^2}{2}E_{1,k+1/2}^{n+1}-\frac{\Delta t\sin(\theta)}{2}\left|\frac{q_eB_{k+1/2}}{m_e}\right\||J_{e_1,k+1/2}^{n+1}|=$$

$$J_{e_1,k+1/2}^n-\frac{\Delta t v_e}{2}J_{e_1,k+1/2}^n+\frac{\Delta t\varepsilon_0\omega_{p_e}^2}{2}E_{1,k+1/2}^n+\frac{\Delta t\sin(\theta)}{2}\left|\frac{q_eB_{k+1/2}}{m_e}\right\||J_{e_1,k+1/2}^n|$$

The same method is then used to find the updating equations for the positive and negative ion plasma. They yield very similar equations:

$$J_{p_1,k+1/2}^{n+1} + \frac{\Delta t \nu_p}{2} J_{p_1,k+1/2}^{n+1} - \frac{\Delta t \varepsilon_0 \omega_{P_p}^2}{2} E_{1,k+1/2}^{n+1} + \frac{\Delta t \sin(\theta)}{2} \left|\frac{q_p B_{k+1/2}}{m_p}\right| |J_{p_1,k+1/2}^{n+1}| =$$

$$J_{p_1,k+1/2}^{n} - \frac{\Delta t \nu_p}{2} J_{p_1,k+1/2}^{n} + \frac{\Delta t \varepsilon_0 \omega_{P_p}^2}{2} E_{1,k+1/2}^{n} - \frac{\Delta t \sin(\theta)}{2} \left|\frac{q_p B_{k+1/2}}{m_p}\right| |J_{p_1,k+1/2}^{n}|$$

$$J_{n_1,k+1/2}^{n+1} + \frac{\Delta t \nu_n}{2} J_{n_1,k+1/2}^{n+1} - \frac{\Delta t \varepsilon_0 \omega_{P_n}^2}{2} E_{1,k+1/2}^{n+1} - \frac{\Delta t \sin(\theta)}{2} \left|\frac{q_n B_{k+1/2}}{m_n}\right| |J_{n_1,k+1/2}^{n+1}| =$$

$$J_{n_1,k+1/2}^{n} - \frac{\Delta t \nu_n}{2} J_{n_1,k+1/2}^{n} + \frac{\Delta t \varepsilon_0 \omega_{P_n}^2}{2} E_{1,k+1/2}^{n} + \frac{\Delta t \sin(\theta)}{2} \left|\frac{q_n B_{k+1/2}}{m_n}\right| |J_{n_1,k+1/2}^{n}|$$

The other current densities 2 and 3 must also be solved for all three of the plasma species. This follows the same method used above. It produces the following equations:

$$J_{e_2,k+1/2}^{n+1} + \frac{\Delta t \nu_e}{2} J_{e_2,k+1/2}^{n+1} - \frac{\Delta t \varepsilon_0 \omega_{P_e}^2}{2} E_{2,k+1/2}^{n+1} - \frac{\Delta t \sin(\theta)}{2} \left|\frac{q_e B_{k+1/2}}{m_e}\right| |J_{e_2,k+1/2}^{n+1}| =$$

$$J_{e_2,k+1/2}^{n} - \frac{\Delta t \nu_e}{2} J_{e_2,k+1/2}^{n} + \frac{\Delta t \varepsilon_0 \omega_{P_e}^2}{2} E_{2,k+1/2}^{n} + \frac{\Delta t \sin(\theta)}{2} \left|\frac{q_e B_{k+1/2}}{m_e}\right| |J_{e_2,k+1/2}^{n}|$$

$$J_{e_3,k+1/2}^{n+1} + \frac{\Delta t \nu_e}{2} J_{e_3,k+1/2}^{n+1} - \frac{\Delta t \varepsilon_0 \omega_{P_e}^2}{2} E_{3,k+1/2}^{n+1} - \frac{\Delta t \sin(\theta)}{2} \left|\frac{q_e B_{k+1/2}}{m_e}\right| |J_{e_3,k+1/2}^{n+1}| =$$

$$J_{e_3,k+1/2}^{n} - \frac{\Delta t \nu_e}{2} J_{e_3,k+1/2}^{n} + \frac{\Delta t \varepsilon_0 \omega_{P_e}^2}{2} E_{3,k+1/2}^{n} + \frac{\Delta t \sin(\theta)}{2} \left|\frac{q_e B_{k+1/2}}{m_e}\right| |J_{e_3,k+1/2}^{n}|$$

$$J_{p_2,k+1/2}^{n+1} + \frac{\Delta t \nu_p}{2} J_{p_2,k+1/2}^{n+1} - \frac{\Delta t \varepsilon_0 \omega_{P_p}^2}{2} E_{2,k+1/2}^{n+1} + \frac{\Delta t \sin(\theta)}{2} \left|\frac{q_p B_{k+1/2}}{m_p}\right| |J_{p_2,k+1/2}^{n+1}| =$$

$$J_{p_2,k+1/2}^{n} - \frac{\Delta t \nu_p}{2} J_{p_2,k+1/2}^{n} + \frac{\Delta t \varepsilon_0 \omega_{P_p}^2}{2} E_{2,k+1/2}^{n} - \frac{\Delta t \sin(\theta)}{2} \left|\frac{q_p B_{k+1/2}}{m_p}\right| |J_{p_2,k+1/2}^{n}|$$

$$J_{p_3,k+1/2}^{n+1} + \frac{\Delta t \nu_p}{2} J_{p_3,k+1/2}^{n+1} - \frac{\Delta t \varepsilon_0 \omega_{P_p}^2}{2} E_{3,k+1/2}^{n+1} + \frac{\Delta t \sin(\theta)}{2} \left|\frac{q_p B_{k+1/2}}{m_p}\right| |J_{p_3,k+1/2}^{n+1}| =$$

$$J_{p_3,k+1/2}^{n} - \frac{\Delta t \nu_p}{2} J_{p_3,k+1/2}^{n} + \frac{\Delta t \varepsilon_0 \omega_{P_p}^2}{2} E_{3,k+1/2}^{n} - \frac{\Delta t \sin(\theta)}{2} \left|\frac{q_p B_{k+1/2}}{m_p}\right| |J_{p_3,k+1/2}^{n}|$$

$$J_{n_2,k+1/2}^{n+1} + \frac{\Delta t\, v_n}{2} J_{n_2,k+1/2}^{n+1} - \frac{\Delta t\, \varepsilon_0 \omega_{p_n}^2}{2} E_{2,k+1/2}^{n+1} - \frac{\Delta t \sin(\theta)}{2} \left| \frac{q_n B_{k+1/2}}{m_n} \right| \left| J_{n_2,k+1/2}^{n+1} \right| =$$

$$J_{n_2,k+1/2}^{n} - \frac{\Delta t\, v_n}{2} J_{n_2,k+1/2}^{n} + \frac{\Delta t\, \varepsilon_0 \omega_{p_n}^2}{2} E_{2,k+1/2}^{n} + \frac{\Delta t \sin(\theta)}{2} \left| \frac{q_n B_{k+1/2}}{m_n} \right| \left| J_{n_2,k+1/2}^{n} \right|$$

$$J_{n_3,k+1/2}^{n+1} + \frac{\Delta t\, v_n}{2} J_{n_3,k+1/2}^{n+1} - \frac{\Delta t\, \varepsilon_0 \omega_{p_n}^2}{2} E_{3,k+1/2}^{n+1} - \frac{\Delta t \sin(\theta)}{2} \left| \frac{q_n B_{k+1/2}}{m_n} \right| \left| J_{n_3,k+1/2}^{n+1} \right| =$$

$$J_{n_3,k+1/2}^{n} - \frac{\Delta t\, v_n}{2} J_{n_3,k+1/2}^{n} + \frac{\Delta t\, \varepsilon_0 \omega_{p_n}^2}{2} E_{3,k+1/2}^{n} + \frac{\Delta t \sin(\theta)}{2} \left| \frac{q_n B_{k+1/2}}{m_n} \right| \left| J_{n_3,k+1/2}^{n} \right|$$

3.4 Creating Matrices

Using these equations, a matrix can be created to solve the system of equations. The process is similar to the rectangular case, but now there are 16 equations and 16 unknowns. Again, A, B and C matrices are defined for the n+1, n, and n+ ½ cases respectively.

$$[A] \cdot \begin{bmatrix} E_r \big|^{n+1} \\ E_1 \big|^{n+1} \\ E_2 \big|^{n+1} \\ E_3 \big|^{n+1} \\ J_{e_r} \big|^{n+1} \\ J_{e_1} \big|^{n+1} \\ J_{e_2} \big|^{n+1} \\ J_{e_3} \big|^{n+1} \\ J_{p_r} \big|^{n+1} \\ J_{p_1} \big|^{n+1} \\ J_{p_2} \big|^{n+1} \\ J_{p_3} \big|^{n+1} \\ J_{n_r} \big|^{n+1} \\ J_{n_1} \big|^{n+1} \\ J_{n_2} \big|^{n+1} \\ J_{n_3} \big|^{n+1} \end{bmatrix} = [B] \cdot \begin{bmatrix} E_r \big|^{n} \\ E_1 \big|^{n} \\ E_2 \big|^{n} \\ E_3 \big|^{n} \\ J_{e_r} \big|^{n} \\ J_{e_1} \big|^{n} \\ J_{e_2} \big|^{n} \\ J_{e_3} \big|^{n} \\ J_{p_r} \big|^{n} \\ J_{p_1} \big|^{n} \\ J_{p_2} \big|^{n} \\ J_{p_3} \big|^{n} \\ J_{n_r} \big|^{n} \\ J_{n_1} \big|^{n} \\ J_{n_2} \big|^{n} \\ J_{n_3} \big|^{n} \end{bmatrix} + [C] \cdot \begin{bmatrix} H_{r_1} \big|^{n+1/2} \\ H_{r_2} \big|^{n+1/2} \\ H_1 \big|^{n+1/2} \\ H_2 \big|^{n+1/2} \\ H_3 \big|^{n+1/2} \\ J_{s_r} \big|^{n+1/2} \\ J_{s_1} \big|^{n+1/2} \\ J_{s_2} \big|^{n+1/2} \\ J_{s_3} \big|^{n+1/2} \end{bmatrix}$$

As with the rectangular case, this equation can be rearranged by moving the A matrix over, creating an equation to calculate the n+1 terms from the known n and n+ ½ terms. This produces the updating equations for each position and time. The coefficients A, B, and C cold be calculated prior to time stepping to improve run time. However, this would be more memory intensive and was not done. Therefore, each coefficient must be calculated at each grid cell and each time step.

$$
\begin{bmatrix}
E_r\big|^{n+1} \\
E_1\big|^{n+1} \\
E_2\big|^{n+1} \\
E_3\big|^{n+1} \\
J_{e_r}\big|^{n+1} \\
J_{e_1}\big|^{n+1} \\
J_{e_2}\big|^{n+1} \\
J_{e_3}\big|^{n+1} \\
J_{p_r}\big|^{n+1} \\
J_{p_1}\big|^{n+1} \\
J_{p_2}\big|^{n+1} \\
J_{p_3}\big|^{n+1} \\
J_{n_r}\big|^{n+1} \\
J_{n_1}\big|^{n+1} \\
J_{n_2}\big|^{n+1} \\
J_{n_3}\big|^{n+1}
\end{bmatrix}
= \left[A^{-1}\right]\cdot\left[B\right]\cdot
\begin{bmatrix}
E_r\big|^{n} \\
E_1\big|^{n} \\
E_2\big|^{n} \\
E_3\big|^{n} \\
J_{e_r}\big|^{n} \\
J_{e_1}\big|^{n} \\
J_{e_2}\big|^{n} \\
J_{e_3}\big|^{n} \\
J_{p_r}\big|^{n} \\
J_{p_1}\big|^{n} \\
J_{p_2}\big|^{n} \\
J_{p_3}\big|^{n} \\
J_{n_r}\big|^{n} \\
J_{n_1}\big|^{n} \\
J_{n_2}\big|^{n} \\
J_{n_3}\big|^{n}
\end{bmatrix}
+ \left[A^{-1}\right]\cdot\left[C\right]\cdot
\begin{bmatrix}
H_{r_1}\big|^{n+1/2} \\
H_{r_2}\big|^{n+1/2} \\
H_1\big|^{n+1/2} \\
H_2\big|^{n+1/2} \\
H_3\big|^{n+1/2} \\
J_{s_r}\big|^{n+1/2} \\
J_{s_1}\big|^{n+1/2} \\
J_{s_2}\big|^{n+1/2} \\
J_{s_3}\big|^{n+1/2}
\end{bmatrix}
$$

As stated previously, these A, B, and C matrices have constant values for each grid cell. Pulling all of the constant terms out of these equations leaves the matrix values:

$$[B]=\begin{vmatrix}
1 & 0 & 0 & 0 & \dfrac{\Delta t}{2\varepsilon_0} & 0 & 0 & 0 & \dfrac{\Delta t}{2\varepsilon_0} & 0 & 0 & 0 & \dfrac{\Delta t}{2\varepsilon_0} & 0 & 0 & 0 \\[2mm]
0 & 1 & 0 & 0 & 0 & \dfrac{\Delta t}{2\varepsilon_0} & 0 & 0 & 0 & \dfrac{\Delta t}{2\varepsilon_0} & 0 & 0 & 0 & \dfrac{\Delta t}{2\varepsilon_0} & 0 & 0 \\[2mm]
0 & 0 & 1 & 0 & 0 & 0 & \dfrac{\Delta t}{2\varepsilon_0} & 0 & 0 & 0 & \dfrac{\Delta t}{2\varepsilon_0} & 0 & 0 & 0 & \dfrac{\Delta t}{2\varepsilon_0} & 0 \\[2mm]
0 & 0 & 0 & 1 & 0 & 0 & 0 & \dfrac{\Delta t}{2\varepsilon_0} & 0 & 0 & 0 & \dfrac{\Delta t}{2\varepsilon_0} & 0 & 0 & 0 & \dfrac{\Delta t}{2\varepsilon_0} \\[2mm]
\dfrac{\Delta t\,\varepsilon_0\omega_{p_e}^2}{2} & 0 & 0 & 0 & 1-\dfrac{\Delta t\,v_e}{2}+|\dfrac{q_e B}{m_e}|\dfrac{\Delta t\sin(\theta)}{2} & 0 & 0 & 0 & 0 & 0 & 0 & 0 & 0 & 0 & 0 & 0 \\[2mm]
0 & \dfrac{\Delta t\,\varepsilon_0\omega_{p_e}^2}{2} & 0 & 0 & 0 & 1-\dfrac{\Delta t\,v_e}{2}+|\dfrac{q_e B}{m_e}|\dfrac{\Delta t\sin(\theta)}{2} & 0 & 0 & 0 & 0 & 0 & 0 & 0 & 0 & 0 & 0 \\[2mm]
0 & 0 & \dfrac{\Delta t\,\varepsilon_0\omega_{p_e}^2}{2} & 0 & 0 & 0 & 1-\dfrac{\Delta t\,v_e}{2}+|\dfrac{q_e B}{m_e}|\dfrac{\Delta t\sin(\theta)}{2} & 0 & 0 & 0 & 0 & 0 & 0 & 0 & 0 & 0 \\[2mm]
0 & 0 & 0 & \dfrac{\Delta t\,\varepsilon_0\omega_{p_e}^2}{2} & 0 & 0 & 0 & 1-\dfrac{\Delta t\,v_e}{2}+|\dfrac{q_e B}{m_e}|\dfrac{\Delta t\sin(\theta)}{2} & 0 & 0 & 0 & 0 & 0 & 0 & 0 & 0 \\[2mm]
\dfrac{\Delta t\,\varepsilon_0\omega_{p_p}^2}{2} & 0 & 0 & 0 & 1-\dfrac{\Delta t\,v_p}{2}-|\dfrac{q_p B}{m_p}|\dfrac{\Delta t\sin(\theta)}{2} & 0 & 0 & 0 & 0 & 0 & 0 & 0 & 0 & 0 & 0 & 0 \\[2mm]
0 & \dfrac{\Delta t\,\varepsilon_0\omega_{p_p}^2}{2} & 0 & 0 & 0 & 1-\dfrac{\Delta t\,v_p}{2}-|\dfrac{q_p B}{m_p}|\dfrac{\Delta t\sin(\theta)}{2} & 0 & 0 & 0 & 0 & 0 & 0 & 0 & 0 & 0 & 0 \\[2mm]
0 & 0 & \dfrac{\Delta t\,\varepsilon_0\omega_{p_p}^2}{2} & 0 & 0 & 0 & 1-\dfrac{\Delta t\,v_p}{2}-|\dfrac{q_p B}{m_p}|\dfrac{\Delta t\sin(\theta)}{2} & 0 & 0 & 0 & 0 & 0 & 0 & 0 & 0 & 0 \\[2mm]
0 & 0 & 0 & \dfrac{\Delta t\,\varepsilon_0\omega_{p_p}^2}{2} & 0 & 0 & 0 & 1-\dfrac{\Delta t\,v_p}{2}-|\dfrac{q_p B}{m_p}|\dfrac{\Delta t\sin(\theta)}{2} & 0 & 0 & 0 & 0 & 0 & 0 & 0 & 0 \\[2mm]
\dfrac{\Delta t\,\varepsilon_0\omega_{p_n}^2}{2} & 0 & 0 & 0 & 1-\dfrac{\Delta t\,v_n}{2}+|\dfrac{q_n B}{m_n}|\dfrac{\Delta t\sin(\theta)}{2} & 0 & 0 & 0 & 0 & 0 & 0 & 0 & 0 & 0 & 0 & 0 \\[2mm]
0 & \dfrac{\Delta t\,\varepsilon_0\omega_{p_n}^2}{2} & 0 & 0 & 0 & 1-\dfrac{\Delta t\,v_n}{2}+|\dfrac{q_n B}{m_n}|\dfrac{\Delta t\sin(\theta)}{2} & 0 & 0 & 0 & 0 & 0 & 0 & 0 & 0 & 0 & 0 \\[2mm]
0 & 0 & \dfrac{\Delta t\,\varepsilon_0\omega_{p_n}^2}{2} & 0 & 0 & 0 & 1-\dfrac{\Delta t\,v_n}{2}+|\dfrac{q_n B}{m_n}|\dfrac{\Delta t\sin(\theta)}{2} & 0 & 0 & 0 & 0 & 0 & 0 & 0 & 0 & 0 \\[2mm]
0 & 0 & 0 & \dfrac{\Delta t\,\varepsilon_0\omega_{p_n}^2}{2} & 0 & 0 & 0 & 1-\dfrac{\Delta t\,v_n}{2}+|\dfrac{q_n B}{m_n}|\dfrac{\Delta t\sin(\theta)}{2} & 0 & 0 & 0 & 0 & 0 & 0 & 0 & 0
\end{vmatrix}$$

35

$$[C]=\begin{vmatrix} 0 & 0 & \dfrac{\Delta t\,\Delta_1}{\varepsilon_0 S} & \dfrac{\Delta t\,\Delta_2}{\varepsilon_0 S} & \dfrac{\Delta t\,\Delta_3}{\varepsilon_0 S} & \dfrac{\Delta t}{\varepsilon_0} & 0 & 0 & 0 \\[2ex] \dfrac{\Delta t}{\varepsilon_0\Delta_1} & \dfrac{\Delta t}{\varepsilon_0\Delta_1} & \dfrac{\Delta t}{\varepsilon_0\Delta_r} & 0 & 0 & 0 & \dfrac{\Delta t}{\varepsilon_0} & 0 & 0 \\[2ex] \dfrac{\Delta t}{\varepsilon_0\Delta_2} & \dfrac{\Delta t}{\varepsilon_0\Delta_2} & 0 & \dfrac{\Delta t}{\varepsilon_0\Delta_r} & 0 & 0 & 0 & \dfrac{\Delta t}{\varepsilon_0} & 0 \\[2ex] \dfrac{\Delta t}{\varepsilon_0\Delta_3} & \dfrac{\Delta t}{\varepsilon_0\Delta_3} & 0 & 0 & \dfrac{\Delta t}{\varepsilon_0\Delta_r} & 0 & 0 & 0 & \dfrac{\Delta t}{\varepsilon_0} \\[1ex] 0 & 0 & 0 & 0 & 0 & 0 & 0 & 0 & 0 \\ 0 & 0 & 0 & 0 & 0 & 0 & 0 & 0 & 0 \\ 0 & 0 & 0 & 0 & 0 & 0 & 0 & 0 & 0 \\ 0 & 0 & 0 & 0 & 0 & 0 & 0 & 0 & 0 \\ 0 & 0 & 0 & 0 & 0 & 0 & 0 & 0 & 0 \\ 0 & 0 & 0 & 0 & 0 & 0 & 0 & 0 & 0 \\ 0 & 0 & 0 & 0 & 0 & 0 & 0 & 0 & 0 \\ 0 & 0 & 0 & 0 & 0 & 0 & 0 & 0 & 0 \\ 0 & 0 & 0 & 0 & 0 & 0 & 0 & 0 & 0 \\ 0 & 0 & 0 & 0 & 0 & 0 & 0 & 0 & 0 \\ 0 & 0 & 0 & 0 & 0 & 0 & 0 & 0 & 0 \\ 0 & 0 & 0 & 0 & 0 & 0 & 0 & 0 & 0 \\ 0 & 0 & 0 & 0 & 0 & 0 & 0 & 0 & 0 \end{vmatrix}$$

Inverting the A matrix would be very difficult and tedious. Instead, the inverse is calculated numerically at each time step for each grid cell. The C matrix is quite sparse; this is because the matrix is associated with the $n + \frac{1}{2}$ terms or the magnetic fields; the current densities for each plasma does not vary directly with the magnetic field.

3.5   Serial Geodesic Model

This system was implemented using the same geodesic grid used by Simpson in [12]. This geodesic grid has several benefits, namely that it includes both topographic and bathymetric data from the NOAA-NGDC "Global Relief CD-ROM".

The grid itself is comprised of 163, 842 grid cells at each radial position. This yields a distance of 62.55 km between grid centers [12]. There are 40 cells radially, making a resolution of 5 km and a total of over 6.5 million cells, the same as [12]. To store the grid in memory, the grid is divided into 5 panels

36

and unwrapped into a flat space. This can be seen in Figure 8. This process also simplifies cell indexing as each panel are the same dimensions and are a Cartesian grid. Reference [12] contains a more detailed analysis of the grid layout.
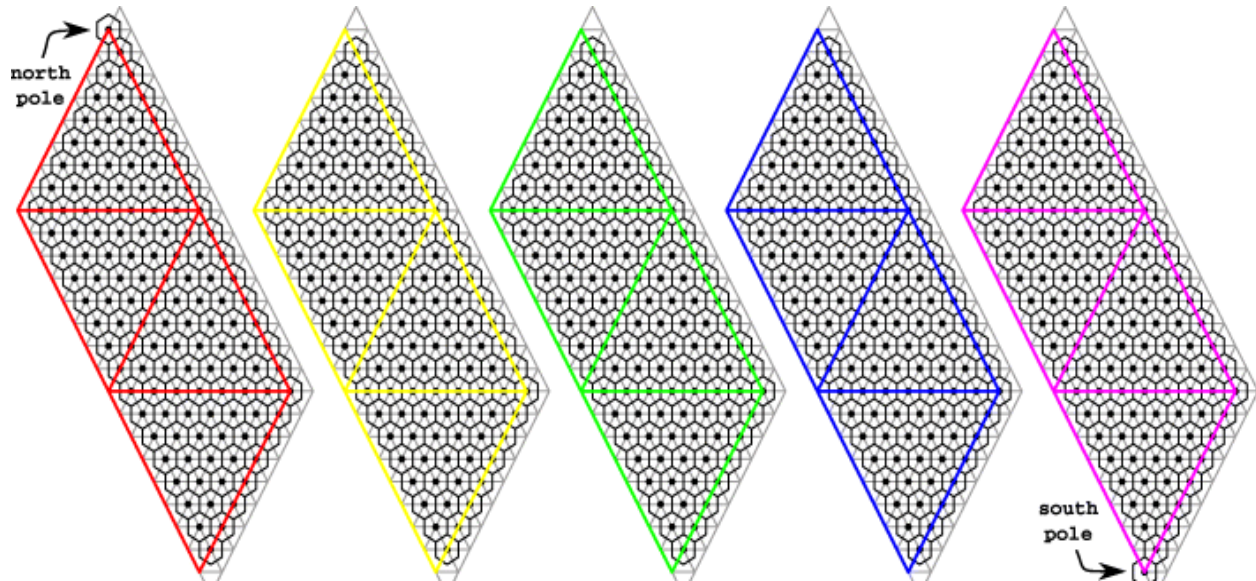
Figure 8: Unwrapped Geodesic Grid [12]

Using the equations derived previously for a magnetized cold plasma, a geodesic grid was obtained that contains the Ionosphere cold plasma model, the topographic data for the surface of the Earth, and the bathymetric data for below the surface. The largest problem with this system is that it is a serial implementation of the grid and does not utilize supercomputing resources or multiple core processors.

Chapter 4

Conclusion

4.1 Summary

FDTD simulations of the Earth-Ionosphere cavity have produced many different results by accounting for different physics in the system. Currently, the 3D Latitude-Longitude grid with a cold plasma Ionosphere contains the most detail. It accounts for varying topography, bathymetry and Ionospheric perturbations [10]. However, the geodesic model offers clear benefits in stability and reduced run times, while retaining the accuracy of the Latitude-Longitude grid.

The equations for a magnetized cold plasma were derived in terms of the geodesic grid. Using these equations, a geodesic model containing topographic, bathymetric, and magnetized cold plasma was created to model the Earth-Ionosphere cavity. The model uses 6.5 million cells for a resolution of 5 km radially and 63 km between adjacent cells. The required simulation time for the serial model makes it infeasible to complete validation.

4.2   Future Work

There are several possibilities for expansion on the existing code. The run time of the current code is a very large issue in any possible future work. The first task would be converting the existing system from a serial code to parallel. A parallel version of the code could reduce run time drastically depending on the hardware. A simple and effective method would be to use MPI which has been used in many other FDTD systems.

After the model has been parallelized, the next step would be to replicate the results of the rectangular coordinate system. Once validated, the model could be used for modeling lightning related Ionospheric phenomena. The model could also be used for modeling long range communications that are effected by the Ionosphere.

References

[1] A. Taflove and S. C. Hagness, *Computational Electrodynamics: The Finite-Difference Time-Domain Method*. Norwood, MA: Artech House Inc, 2005.

[2] J.J. Simpson. "Current and Future Applications of 3-D Global Earth-Ionosphere Models Based on the Full-Vector Maxwell's Equations FDTD Method". *Surveys in Geophysics*, vol. 30, pp 105-130, March 2009.

[3] M. Thevenot, et al. "A FDTD scheme for the computation of VLF-LF propagation in the anisotropic earth-ionosphere waveguide". *Ann. Telecommun*, vol 54, pp 297-310, 1999.

[4] S. A. Cummer. "Modeling Electromagnetic Propagation in the Earth-Ionosphere Waveguide". *IEEE Transactions on Antennas and Propagation*, vol. 48, no. 9, September 2000.

[5] K. G. Budden, "The Constitutive Relations" in *The Propagation of Radio Waves: The Theory of Radio Waves of Low Power in the Ionosphere and Magnetosphere*, Cambridge, England: Cambridge University Press, 1985, ch 3, sec. 3.6, pp 45.

[6] J. J. Simpson, A. Taflove. "Global Three-Dimensional FDTD Modeling of Impulsive ELF Propagation About the Earth". *Antennas and Propagation Society International Symposium, 2003. IEEE*, vol. 4, pp 940-943, June 2003.

[7] J. J. Simpson, A. Taflove. "Three-Dimensonal FDTD Modeling of Impulsive ELF Propagation About the Earth-Sphere". *IEEE Transactions on Antennas and Propagation*, vol 52, February 2004.

[8] P. R. Bannister. "The determination of representative ionospheric conductivity parameters for ELF propagation in the Earth-ionosphere waveguide". *Radio Science*, vol 20, no 4, pp 977-984, August 1984.

[9] P. R. Bannister. "ELF Propagation Update". *IEEE Journal of Oceanic Engineering*, vol OE-9, no 3, pp 179-188, July 1984.

[10] Y. Yu and J.J. Simpson. "An E-J Colocated 3-D FDTD Model of Electromagnetic Wave Propagation in Magnetized Cold Plasma". *IEEE Transactions on Antennas and Propagation*, vol. 58, no. 2, February 2010.

[11] H.G. Booker. *Cold Plasma Waves*. The Netherlands: Martinus Nijhouf, 1984.

[12] J.J. Simpson, R.P. Heikes, and A. Taflove. "FDTD Modeling of a Novel ELF Radar for Major Oil Deposits Using a Three-Dimensional Geodesic Grid of the Earth-Ionosphere Waveguide". *IEEE Transactions on Antennas and Propagation*, vol. 54, no. 6, June 2006.

[13] NOAA-NGDC, Global Relief CD-ROM.

[14] Y. Wang, Q. Cao, and B. Su. "Spatial Stability Analysis for the Geodesic FDTD Algorithm". *IEEE*

International RF and Microwave Conference, Seremban, Malaysia, 2011.

[15] Y. Wang, H. Xia, and Q. Cao. "Analysis of ELF Attenuation Rate Using the Geodesic FDTD Algorithm". *Microwave and Millimeter Wave Technology (ICMMT), 2010 International Conference on*, May 2010.

[16] M. J. S. Johnston. "Review of Electric and Magnetic Fields Accompanying Seismic and Volcanic Activity." *Surveys in Geophysics*, vol 18, pp 441-476, 1997.

[17] J. J. Simposn, A Taflove. "Electrokinetic effect of the Loma Prieta earthquake calculated by an entire-Earth FDTD solution of Maxwell's equations". *Geophysical Research Letters*, vol 32, 2005.

[18] J. J. Simpson. "Global FDTD Maxwell's Equations Modeling of Electromagnetic Propagation From Currents in the Lithosphere". *IEEE Transactions on Antennas and Propagation*, vol 56, January 2008.

[19] A. C. Fraser-Smith et al. "Low-frequency magnetic field measurements near the epicenter of the Ms 7.1 Loma Prieta Earthquake". *Geophysical Research Letters*, vol 17, no 9, pp 1465-1468, 1990.

[20] K.S. Yee. "Numerical Solution of Initial Boundary Value Problems Involving Maxwell's Equations in Isotropic Media". *IEEE Transactions on Antennas and Propagation*, vol. 14, 1966.